JOURNAL OF PETROLOGY

Journal of Petrology, 2018, 1–29
doi: 10.1093/petrology/egy094
Advance Access Publication Date: 15 October 2018
Original Article

OXFORD

Mechanical Mixing of Garnet Peridotite and Pyroxenite in the Orogenic Peridotite Lenses of the Tvaerdal Complex, Liverpool Land, Greenland Caledonides

Hannes K. Brueckner[1,2]*, L. Gordon Medaris, Jr[3], William L. Griffin[4], Scott M. Johnston[5], Ebbe H. Hartz[6], Norman Pearson[4], Yue Cai[1] and Arild Andresen[7]

[1]Lamont-Doherty Earth Observatory of Columbia University, 61 US-9W Palisades, NY 10964, USA; [2]The CUNY Graduate Center and School of Earth and Environmental Sciences, Queens College, 65-21 Main St. Flushing, NY 11367, USA; [3]Department of Geoscience, University of Wisconsin-Madison, Madison, WI 53706, USA; [4]Department of Earth and Planetary Sciences, Australian Research Council Centre of Excellence for Core to Crust Fluid Systems (CCF)/(GEMOC), Macquarie University, NSW 2109, Australia; [5]Physics Department, California Polytechnic State University, San Luis Obispo, CA 93407, USA; [6]Centre for Earth Evolution and Dynamics, Department of Geosciences, Oslo University, P.O. Box 1028 Blindern, 0316 Oslo, Norway; [7]Department of Geosciences, University of Oslo, P.O. Box 1047 Blindern, 0316 Oslo, Norway

*Corresponding author. P.O. Box 1000, 61 Route 9W, Palisades, NY 10964-1000 USA, Telephone: (845) 359-2000. Fax: (845) 365-8150. E-mail: Hannes@ldeo.columbia.edu

Received April 9, 2018; Accepted September 28, 2018

ABSTRACT

The Tvaerdal Complex is an eclogite-bearing metamorphic terrane in Liverpool Land at the southern tip of the Greenland Caledonides. It is a Baltic terrane that was transferred to Laurentia during the Scandian orogeny. It exposes a few small garnet dunite and harzburgite lenses, some containing parallel layers of garnet pyroxenite and peridotite (including lherzolite). Sm–Nd mineral ages from the pyroxenites indicate recrystallization occurred at the same time (≈405 Ma) as eclogite recrystallization in the enclosing gneiss. Geothermobarometry indicates these eclogites and pyroxenites shared a similar pressure-temperature history. This congruent evolution suggests pyroxenite-bearing peridotite lenses were introduced from a mantle wedge into subducted Baltic continental crust and subsequently shared a common history with this crust and its eclogites during the Scandian orogeny. Some garnet peridotite samples contain two garnet populations: one Cr-rich (3·5–6·2 wt % Cr_2O_3) and the other Cr-poor (0·2–1·4 wt %). Sm–Nd analyses of two such garnet peridotites define two sets of apparent ages: one older (>800 Ma) for Cr-rich garnets and the other younger (<650 Ma) for Cr-poor garnets. We propose that the younger Cr-poor garnets were derived from fractured and disaggregated garnet pyroxenite layers (i.e. are M_2) and were mixed mechanically with older (i.e. M_1) garnets of the host peridotite during intense Scandian shearing. Mechanical mixing may be an important mantle process.

Key words: orogenic peridotite; mechanical mixing; pyroxenite; peridotite, Greenland Caledonides

INTRODUCTION

Liverpool Land (LL) at the southern end of the Greenland Caledonides is a crystalline terrane comprised of plutonic rocks in the north and metamorphic rocks in the south (Fig. 1). The metamorphic rocks include numerous eclogites (Augland *et al.*, 2010; Johnston *et al.*, 2010; Corfu & Hartz, 2011) and a few, small (≈decametre) peridotite lenses that locally are

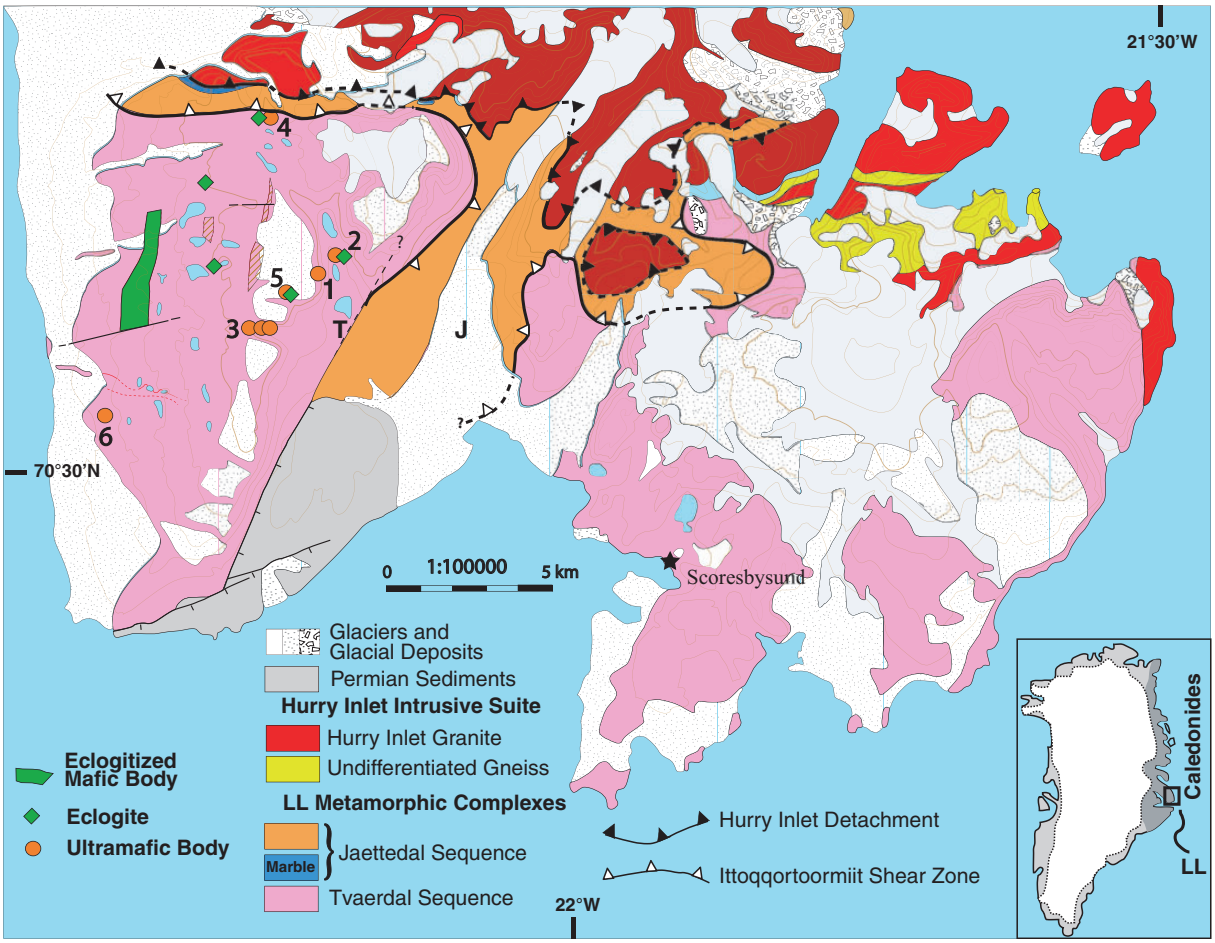

Fig. 1. Map of the Liverpool Land (LL) metamorphic terrane showing the Tvaerdal and Jaettedal metamorphic complexes, major tectonic features (from Johnston *et al.*, 2010) and locations of peridotite lenses (circles) and eclogites (diamonds). Sample numbers refer to peridotite localities in Table 1. Geographic coordinates of most peridotite lenses are given in Table 1. T and J are the valleys called Tvaerdal and Jaettedal.

garnetiferous (Augland *et al.*, 2011). Augland *et al.* (2010) proposed that the entire metamorphic terrane be called the Liverpool Land Eclogite Terrane (LLET). They proposed further that the LLET was a Baltic, rather than Laurentian, terrane (see also Smith & Cheeney, 1981) that became stranded on the Greenland side of the Caledonides during the opening of the Atlantic. Subsequent work has confirmed the Scandian (411–398 Ma) evolution of the eclogites and the Baltic origin of the gneisses that host them (Johnston, *et al.*, 2010; Augland *et al.*, 2011; Corfu & Hartz, 2011; Brueckner *et al.*, 2016). However, mapping by Johnston *et al.* (2010) showed that the metamorphic rocks are not a single high pressure/ultrahigh pressure (HP/UHP) complex, but rather two complexes, with the eclogites, peridotites and their host rocks comprising a Baltican HP/UHP terrane, the Tvaerdal Complex and the rest of the metamorphic rocks forming a Laurentian granulite facies terrane, the Jaettedal Complex.

This division into a Baltic Complex (Tvaerdal) and a Laurentian Complex (Jaettedal) resolves the problem of how the peridotite lenses came to be embedded in the southernmost Greenland Caledonides. The Scandian Orogeny is generally modeled by the westward (present coordinates) subduction of Baltica (Scandinavia) beneath Laurentia (Greenland) (Krogh, 1977; Andersen *et al.*, 1991; see also Brueckner & Van Roermund, 2004; Hacker *et al.*, 2010; Gee *et al.*, 2012 for recent reviews). If the Tvaerdal Complex were a Laurentian terrane, the peridotite bodies within it would have had to move upward into the overlying plate. But if the Tvaerdal Complex was part of Baltica when it subducted beneath Laurentia, it could have picked up the peridotite fragments from the overlying Laurentian mantle wedge (Brueckner & Medaris, 2000). A contrary view to the mantle subduction model is, however, held by one of us (see Hartz *et al.*, 2005, 2007). Models in which the peridotites were derived from the Baltic rather than Laurentian mantle have been presented by Terry *et al.* (1999) and Majka *et al.* (2014).

To test the possibility that the Tvaerdal Complex is a Baltic terrane, and the peridotites within it have a Laurentian affinity, seven of the known peridotite bodies in Liverpool Land, as well as peridotite and pyroxenite blocks in glacial till, were investigated. The major, minor and trace element compositions of

peridotite and pyroxenite whole-rock samples, as well as the compositions of their constituent minerals were determined. Electron microprobe scans were recorded across key minerals. Pressure-temperature (*P–T*) equilibration conditions and Sm–Nd mineral ages were determined from selected samples and compared with published pressure-temperature-time (*P–T–t*) information from the associated Tvaerdal eclogites and host gneisses. Re–Os isotopic data from sulfides are also presented for selected samples.

The study became complicated when we observed that some garnet peridotites contain garnets with variable Cr concentrations, which, in at least one case could be divided into two distinct populations: Cr-rich and Cr-poor. Sm–Nd results from two other peridotites indicate that their garnets formed or re-equilibrated during two separate metamorphic events. Thus some peridotites contain two garnet populations and we present evidence that they might have been mixed together mechanically. Mechanical mixing may be an underappreciated process that could play an important role in mantle evolution.

REGIONAL SETTING

The Greenland Caledonides

The southern half of the Greenland Caledonides is composed of west vergent nappe complexes in the west and crystalline complexes, including LL, to the east (Gee *et al.*, 2008, 2012; Higgins *et al.*, 2008; Gasser, 2014). The allochthons are separated from LL by 100 km of post-orogenic rift deposits, but LL is generally considered to be tectonically positioned below these allochthons and to represent the deepest tectonic level of the Greenland Caledonides, similar in tectonic position to the Western Gneiss Complex (WGC) of the Norwegian Caledonides.

The Liverpool Land Metamorphic Terrane

Liverpool Land is the southernmost exposed crystalline terrane of the Greenland Caledonides (Fig. 1), covered to the south by the fjord Scorsbysund and by Mesozoic sedimentary sequences. Cheeney (1985) divided the crystalline rocks into a northern, largely igneous complex, the Hurry Inlet Plutonic Terrane and a southern metamorphic complex (Fig. 1). The shallowly north-dipping Gubbedalen Shear Zone (aka Hurry Inlet Detachment) with top to the north kinematic indicators separates the two complexes (Augland *et al.*, 2010; Johnston, *et al.*, 2010). The Hurry Inlet plutonic Complex is composed of calc-alkaline intrusives with screens and enclaves of Proterozoic supracrustal rocks (Coe, 1975; Johnston *et al.*, 2010; Corfu & Hartz, 2011; Augland *et al.*, 2012). The plutons have been dated between 475 to 415 Ma (Corfu & Hartz, 2011; Augland *et al.*, 2012; Brueckner *et al.*, 2016) and probably represent deep intrusive levels of a continental arc complex that developed on the eastern margin of Laurentia during the closure of Iapetus.

As noted above, Johnston *et al.* (2010) concluded that the eclogites and peridotites within the metamorphic complex are restricted to a tectonically lower orthogneiss sequence (the Tvaerdal Complex) separated by another shear zone (the Ittoqqortoormiit shear zone) from a tectonically higher eclogite-free unit containing predominant orthogneiss and subordinate granulite, pelitic schist, calc-silicate rocks and marble (the Jaettedal Complex). Zircon cores from the Jaettedal Complex give Archean and Mesoproterozoic U–Pb ages, while zircon cores from the Tvaerdal Complex give Mesoproterozoic ages only. The Jaettedal Complex underwent granulite facies metamorphism and melting between 460 and 410 Ma (Johnston *et al.*, 2010, 2015), whereas the peak metamorphic history of the Tvaerdal Complex occurred between 412–395 Ma (see below). Thus the two complexes had different Precambrian histories and were metamorphosed at different grades and at different times, providing compelling evidence that the two complexes originated from Laurentia and Baltica, respectively. This subdivision requires further evaluation, but in the meantime we suggest that the two metamorphic complexes should be called collectively the LL Metamorphic Terrane, with eclogite-facies HP/UHP metamorphism restricted to the Tvaerdal Complex.

Together the Hurry Inlet Plutonic Terrane and Jaettedal Complex represent deep levels of a Laurentian continental arc complex that was active during the closure of Iapetus, while the Tvaerdal Complex was a fragment of the approaching Baltic passive margin. Igneous activity within this arc complex ended, and metamorphism of the Tvaerdal Complex began, when Baltica and Laurentia collided and the Tvaerdal Complex was subducted into the mantle beneath Laurentia. There, the Tvaerdal Complex underwent HP/UHP metamorphism and collected fragments of peridotite from the overlying mantle wedge. The Tvaerdal and Jaettedal Complexes were subsequently juxtaposed along the Ittoqqortoormiit shear zone as the Tvaerdal Complex was exhumed from the upper mantle. This juxtaposition occurred in the lower to middle crust (Johnston *et al.*, 2015) at approximately 395 Ma. Finally, as a composite metamorphic terrane (i.e. the LL Metamorphic Terrane), they shared a common retrograde and melting history while they were exhumed towards the surface along the Grubbedalen shear zone between 395–360 Ma (Augland *et al.*, 2010).

Eclogites of the Tvaerdal complex

Eclogites in Liverpool Land were first reported by Sahlstein (1935). They occur as metre-scale boudins and boudin trains and as portions of decametre to kilometre-scale mafic lenses and layers. Most eclogites are massive and medium grained and contain omphacite + garnet ± quartz while some are layered, coarse grained and commonly contain orthopyroxene ± biotite in addition to garnet and omphacite. Further details can

be found in Augland *et al.* (2010, 2011), Johnston *et al.* (2010) and Corfu & Hartz (2011). Brueckner *et al.* (2016) calculated peak metamorphic conditions of 800–900°C and 35–40 kbar. Peak metamorphism was followed by nearly isothermal decompression to ~16 kbar and ~800°C. Dating by a variety of techniques indicate that UHP metamorphism occurred between 412–395 Ma followed by retrograde metamorphism and anatectic melting between 395–375 Ma (Augland *et al.* 2010; Corfu & Hartz, 2011; Brueckner *et al.*, 2016). Taken together, the very consistent ages confirm that HP/UHP metamorphism of the Tvaerdal Complex was essentially simultaneous with peak HP/UHP metamorphism in the WGC of the Norwegian Caledonides during the Scandian orogeny.

TVAERDAL PERIDOTITES AND PYROXENITES

Field relationships

Peridotite and pyroxenite were first reported in Liverpool Land as blocks in glacial deposits by Smith & Cheeney (1981) and Cheeney (1985). Smith & Cheeney (1981) noted the unusually high Cr contents of garnet and clinopyroxene in one of them. There were no reports of peridotite in outcrop until field parties led by Ebbe Hartz in 2005 and 2006 and Hannes Brueckner and Scott Johnston in 2009 located seven small (m–dm) peridotite bodies (open circles in Fig. 1). Most occurrences are moderately to pervasively serpentinized and only three (Fig. 1 and Table 1: locations 1, 2 and 5) provided samples with sufficient unaltered clinopyroxene and garnet to warrant Sm–Nd analyses. Augland *et al.* (2011) described another peridotite lens (map location 6) with unaltered clinopyroxene and garnet and samples from that lens (LEA 08–04 and AA 08–47) were donated for this study. We also collected additional relatively unaltered samples from talus (HKB-6P, LM-42A LM-42B and LM-43) and from till (HKB Camp 1–1, HKB Camp 2–1; Table 1). Some important data are from these samples.

All peridotite bodies exposed in outcrop are relatively small concordant lenses a metre to a few metres wide and metres to tens of metres long (Fig. 2a). They are (or were prior to serpentinization) dominantly fine- to medium-grained dunite or harzburgite (olivine ± orthopyroxene) commonly containing dispersed, easily visible (2–30 mm), partially to completely kelyphitized garnets (Fig. 2b). A few bodies are strikingly layered, defined by parallel garnet-rich and garnet-poor dunite (Fig. 2c), pyroxenite and lherzolite layers (Fig. 2d and e). Some garnet-rich layers are thin, locally one or two grains wide, with the garnets separated from each other by recrystallized olivine (Fig. 2d, left side; see also Augland *et al.*, 2011, Fig. 3). Three lenses contain 0·5–10 cm thick garnet and clinopyroxene-rich layers of garnet pyroxenite, garnet wehrlite and garnet lherzolite (Fig. 2c and d). These layers are parallel to the overall foliation, which, in turn is concordant or nearly concordant to the enclosing gneissic foliation. The striking parallelism of this fabric is believed to be the result of intense shear and/or shortening (Fig. 2 c, d and f). Amphibole-bearing kelyphite reaction rims around garnets are locally stretched out into this planar fabric (Fig. 2f) indicating that some deformation occurred within the crust during retrogression under amphibolite facies conditions. Folds were not found in any of the peridotite bodies.

Penetrative, parallel, thin serpentinite veins crosscut the earlier compositional banding in most lenses. The serpentinite veins consist of serpentine (largely chrysotile) and trains of opaque minerals, presumably Fe-oxides, which initially segment olivine grains into aligned micro-ellipses and rectangular blocks before they are completely replaced by serpentine. Some lenses contain additional cross-cutting planar fabrics defined by serpentine + oxides.

Petrography

Initial mineral proportions were calculated for most samples (Table 1) based on their bulk composition and the assumption that the assemblages consisted of variable proportions of olivine, orthopyroxene, clinopyroxene and garnet. These abundances were used to divide the samples into different peridotite and pyroxenite classes. The observed abundances of retrograde minerals, such as amphibole and opaque minerals are noted in parentheses in Table 1. The calculated modes reveal a spectrum of rock types including dunite, harzburgite, lherzolite, wehrlite, olivine websterite, websterite and clinopyroxenite (Table 1). We suspect that some olivine-rich assemblages, such as the lherzolites, resulted from mechanical mixing rather than through some chemical or magmatic process. We present evidence for this suspicion throughout the manuscript.

Dunites and harzburgites display a 0·5–2·0 mm granoblastic assemblage of olivine ± orthopyroxene ± clinopyroxene ± amphibole ± spinel and scattered, larger (2–30 mm) grains of garnet (Fig. 2 b, g and h). Lattice preferred orientation (LPO) fabrics for LM-42B (Luc Mehl, personal communication) give [001](100) (C-type) patterns for olivine and a [001](100) pattern for orthopyroxene. These patterns indicate olivine and orthopyroxene underwent dynamic recrystallization while undergoing large strains (Wang *et al.*, 2013), while mechanically stronger garnet resisted recrystallization.

Garnet lherzolite, olivine websterite and wehrlite form 0·5 to 10 cm thick layers within dunite and harzburgite (Fig. 2d, e and h) and are texturally similar, with a relatively fine grained olivine matrix (0·5–1·0 mm) enclosing larger grains of orthopyroxene, clinopyroxene (1·0–3·0 mm) and garnet (2.0–30 mm). The size range for the garnet is particularly striking (Fig. 2 g and h). Especially notable are garnets in some samples (e.g. LM-42B; Fig. 2g) that show considerable colour variations in plane light, ranging from a deep red or violet to orange to light pink. The differently coloured garnets are randomly distributed in some samples (LM-42B) while in others the lighter garnets are concentrated in

Table 1: Peridotite and pyroxenite localities and calculated modes, Tvaerdal Complex, Liverpool Land

Map	Sample #	Grt bearing #	Coordinates rock type	ol	opx	cpx	grt	amp	op	other	comment
1.	LM-38	Clinopyroxenite	N70.56, W22.18	<1	0	40	60	(40)	(5)	tr green sp, bi	fragmented grt
2.	HKB 2A	Dunite	Tvaerdal	92	5	0	3		(10)	5% bi	grt completely kely
	HKB 2B	Websterite	N70.56, W22.18	0	37	22	41	(2)	(5)	dark & pale grts	7 cm thick dike
	HKB 2C	Ol-Websterite	Tvaerdal	25	16	29	30				cpxite-dunite contact
3.	HKB 3	Lherzolite	Núkaitsoq N70.54, W22.25	46	14	19	20	(7)		37% serp	kely largely amph
4.	HKB 4	Dunite	Gubbedal N70.60, W22.22	87	8	1	4	(8)	(2)	3% kely	
5.	EH-21A	Lherzolite	Tvaerdal	50	11	13	26	(15)		5% kely	30% serp
	EH-21B	Harzburgite	N70.55, W22.21	69	27	0	4				1.5 cm grt pclast
	EH-22	Wehrlite	Tvaerdal	48	2	31	19	(10)		dark & pale grts	30% serp
6.	LEA 08–04	Peridotite	N70.503, W22.34	nd	nd	nd	nd	nd			see Augland *et al.* 2011
	AA 08–47	Pyroxenite	N70.503, W22.34	nd	nd	nd	nd	nd			see Augland *et al.* 2011
—	Camp 1–1	Harzburgite	block in till	68	31	0	1		(8)	sp	90% serp
—	Camp 2-1A	Lherzolite	block in till	50	15	29	7		tr	tr sp	4 cm thick in dunite
—	Camp 2-1B	Lhrz-Dun contact		–	–	–	–				partially disaggretated
—	Camp 2–2	Dunite	block in till	83	9	0	8				
—	LM-42A	Harzburgite	talus below 1	78	15	2	6	(tr)	(2)	2% kely	40% serp
	LM-42B*	Lherzolite	(≈N70.56, W22.17)	57	10	12	10	7	2	2% sp, 8% kely	Cr rich & Cr poor grt
—	LM-43	Websterite	Talus below 1.	0	27	19	55	(10)			5cm thick vein in dunite
—	HKB-6P	Harzburgite	talus below 5	84	12	0	3				grt in single grain layers

The first column lists the sample locations shown in Fig. 1. Most modes were calculated from the anhydrous rock compositions recalculated to 100% (Table 2). Numbers in parenthesis are hydrous minerals and oxides present in thin section.
*Whole-rock not analysed; abundance estimated from thin section.
ol, olivine; opx, orthopyroxene; cpx, clinopyroxene; grt, garnet; amp, amphibole; op, opaques; sp, spinel; kely, kelyphyte; serp, serpentinite.

thin (mm scale) zones (Fig. 2h). These colour differences are also obvious in mineral separates viewed beneath a binocular microscope. The colour variations are primarily the result of different Cr contents, which range from 0·2 to 6·3 wt % in sample LM-42B. Some garnet grains are blocky, angular or irregular in outline rather than equant granoblastic (Fig. 2g and h), as if the garnets had been mechanically fragmented prior to kelyphitization. Many grains contain internal planar cracks that are locally offset by other fractures. Garnets in other thin sections of both pyroxenite (Fig. 2i, j and k) and peridotite (Fig. 2m) are fractured and locally detached and separated, again suggesting mechanical breakdown.

All garnet grains in the peridotites are partly to completely replaced by kelyphite consisting of radially arranged fibres of orthopyroxene, spinel and amphibole (Fig. 2n and o). Some kelyphites display a thin, discontinuous outer rim of orthopyroxene against the kelyphite, which in turn is enclosed by a zone of coarse grained amphibole (similar to textures described by Obata, 2011). The amphibole locally has a vermicular structure where it borders the kelyphite and in some cases is optically continuous with amphibole threads within the kelyphite. Amphibole also occurs as isolated grains within the rock matrix. One garnet in LM-42B (Fig. 2o) displays two reactions rims around a Cr-rich grain: an inner one composed of Cr-poor garnet and spinel (bottom of grain) and an outer one of orthopyroxene, spinel and amphibole. It is likely the strong development of the outer rim destroyed evidence for the inner rim in most garnets.

Pyroxenites include garnet websterite and clinopyroxenite and are composed of medium grained (2·0–5·0 mm) granoblastic garnet + clinopyroxene ± orthopyroxene. Most pyroxenites contain little or no olivine (0–10%; Fig. 2j and l) except for olivine websterite sample HKB-2C which has 25%. Amphibole occurs in most samples, ranging from 2 to 40% and two samples contain biotite, one with ≈5%. Textures of the hydrous phases indicate that they are retrograde.

Whole-rock chemistry

Major elements

Whole-rock major element compositions of Tvaerdal peridotite and pyroxenite samples were determined by XRF. Analytical techniques are described in Supplementary Data Table S1 (Supplementary Data are available for downloading at http://www.petrology.oxfordjournals.org). Averaged compositions are listed in Tables 2 (major elements) and 3 (trace elements; complete data in Supplementary Data Table S2). Serpentinization and the resultant production of iron oxides has perturbed the chemistry of most samples; thus the analyses are recalculated to 100% on an anhydrous basis, with all Fe reported as FeO. Based on the proportions of olivine, orthopyroxene, and clinopyroxene, the analysed Tvaerdal ultramafic suite includes three samples of dunite, four harzburgites, three lherzolites, one wehrlite, one olivine websterite, two websterites and one clinopyroxenite (Fig. 3).

A plot for selected major element abundances vs MgO concentration is presented in Fig. 4 in which

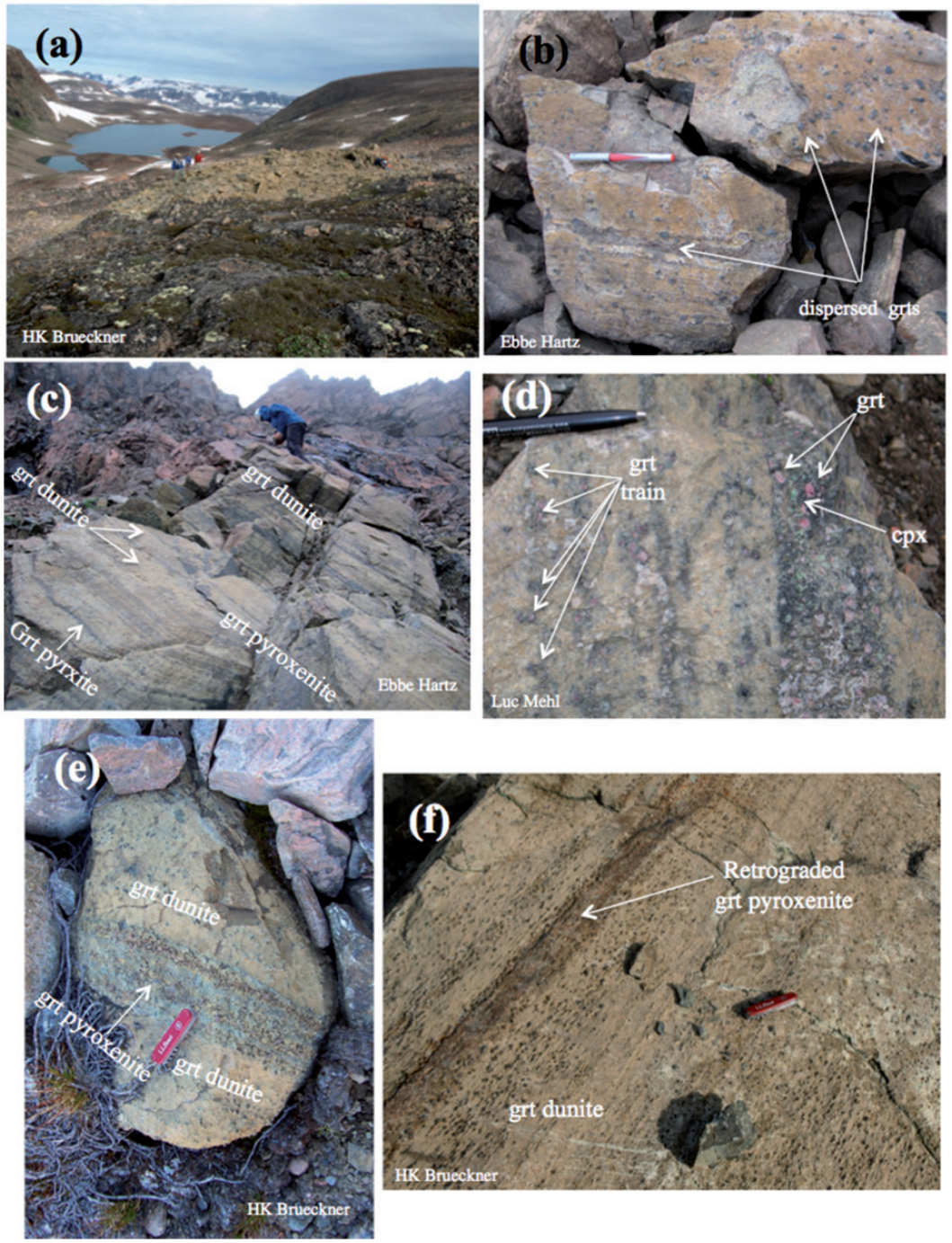

Fig. 2. (a) Typical peridodite lens within gneisses of the Tvaerdal Complex. (b) Loose block of garnet dunite showing scattered M_1 garnets. (c) Peridotite lens EH-22 with strikingly parallel garnet dunite, garnet pyroxenite and garnet-train layers of varying thickness. (d) Close up of the peridotite shown in (c). Garnet wehrlite (EH-22) was sampled from the thick layer on the right. The thin parallel dark layers are garnet-rich trains. The dark colour is the result of kelyphite formation and preferential serpentinization. Note the colour variation in garnets. (e) Loose boulder showing pyroxenite layer in garnet dunite with scattered M_1 garnets. (f) Pyroxenite layer within dunite. Sheared out kelyphite reaction rims around M_1 garnets define a parallel planar fabric. (g) Thick section of lherzolite LM-42B showing two garnet generations; one Cr-rich (dark), the other Cr-poor (light). The yellow lines show scans GM 1 and GM 2 in Fig. 9. (h) Polished slab of wehrlite EH-22 with partially disaggregated garnet-clinopyroxene rich layer. Again, note colour variations in the garnets. (i) Thin section of garnet pyroxenite LM-38 showing evidence of fracturing and disaggregation. (j) Thin section of garnet websterite HKB-2B showing evidence of fracturing and disaggregation. (k) Backscattered electron image of a garnet in HKB-2B showing asymmetrical Cr zoning. Two small grains appear to be in the process of breaking away from the larger grain. (l) Thin section of a portion of garnet websterite HKB-2B showing a relatively coherent granoblastic fabric. (m) Garnet harzburgite EH-21B showing fragmented and partially detached garnets in an olivine-rich matrix. (n) Kelyphite reaction rim composed of amphibole and spinel around garnet. The kelyphite in turn is partially enclosed by coarser amphibole grains. (o) Electron microprobe image of garnet 1 in LM-42B (Fig. 2g) showing an inner kelyphite composed of spinel and low-Cr garnet (bottom) and an outer kelyphite composed of spinel, orthopyroxene and amphibole.

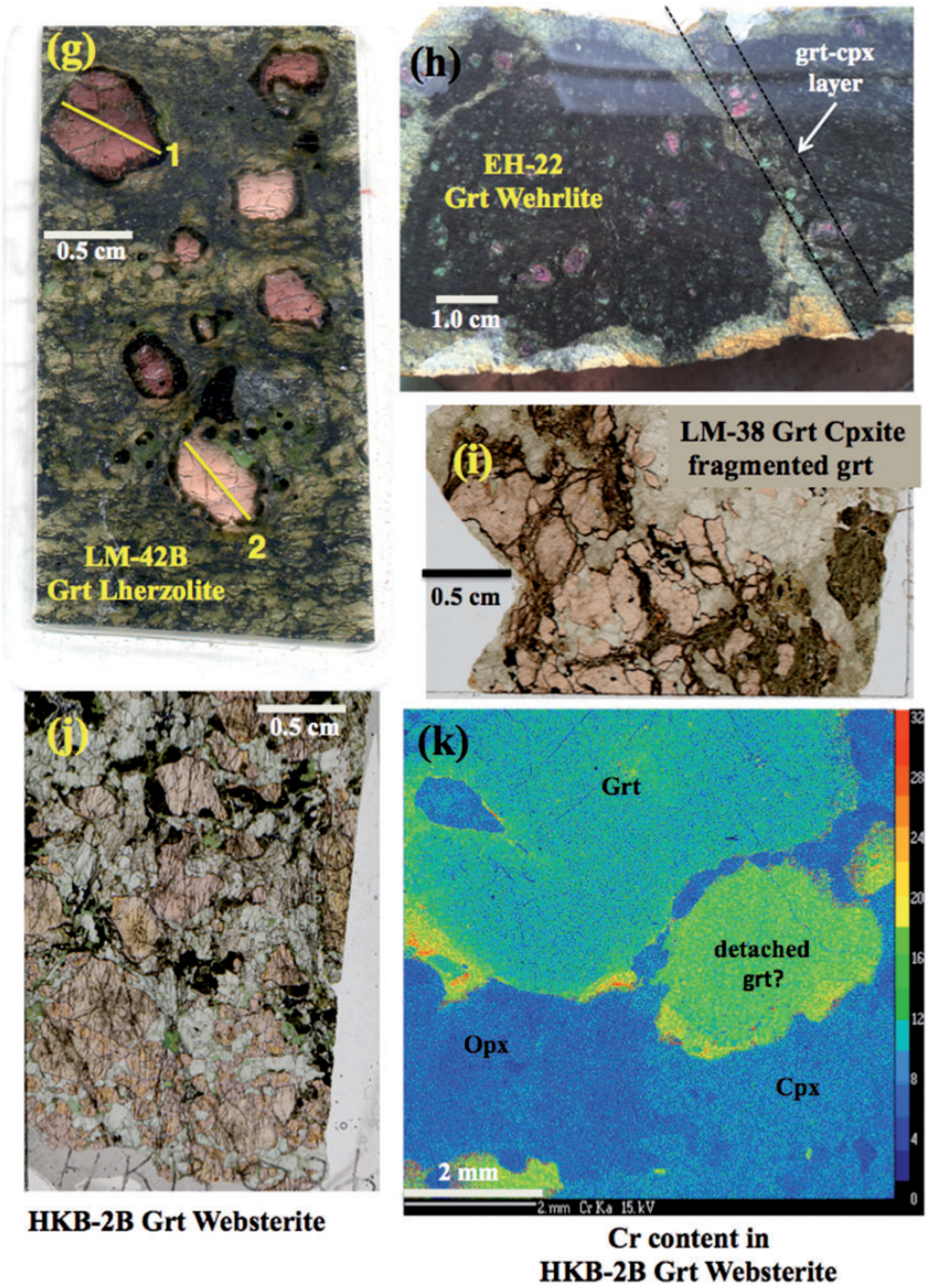

Fig. 2. Continued

compositions of the Tvaerdal peridotites and pyroxenites are compared to those from the WGC of the Norwegian Caledonides (Supplementary Data Table S2a). The LL peridotite and pyroxenite suite shows a pattern of chemical variation with respect to wt % MgO that is common in such suites worldwide (Bodinier & Godard, 2004); namely, an increase in MgO is accompanied by a pronounced decrease in TiO_2, Al_2O_3, and CaO, with a lesser decrease in SiO_2 and FeO, and an increase in NiO and Cr_2O_3. In detail, the LL suite consists of three chemical groups of rocks: seven samples of strongly depleted dunite and harzburgite that contain >45% MgO, three samples of lherzolite and one of wehrlite that cluster around the composition of Primitive Mantle (McDonough & Sun, 1995) and four samples of pyroxenite that contain <30% MgO.

Although the lherzolite and wehrlite samples generally plot in the vicinity of Primitive Mantle, their compositions are highly variable, particularly for TiO_2, Al_2O_3, Cr_2O_3 and CaO, which have relative standard deviations of 72, 29, 75, and 59%, respectively. Interestingly, the data from the WGC shows, with two exceptions, a gap from 31 to 39% MgO between the pyroxenites and peridotites. The three LL lherzolites (EH-21A, HKB-3 and

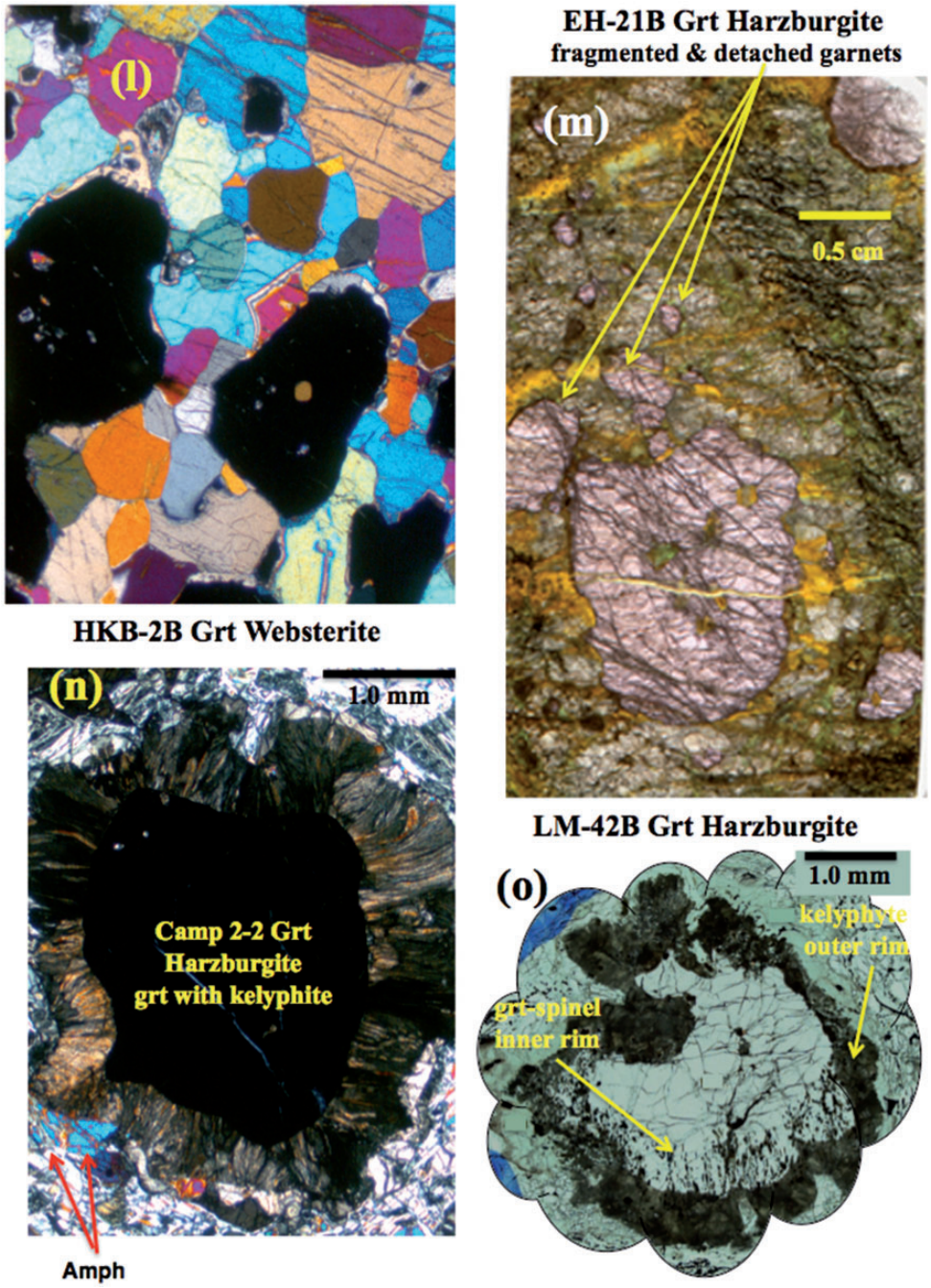

Fig. 2. Continued

Camp 2–1) and one wehrlite (EH-22), fall into this gap (Fig. 4).

Trace elements

The compatible element Ni decreases, and the incompatible elements V, Y and Sr increase systematically with decreasing MgO (Fig. 5); such patterns are consistent with enrichment of highly depleted mantle through the introduction of a pyroxenitic component. Zr and Ba also show a tendency to increase with a decrease in MgO, although with much greater scatter than in the other incompatible elements.

Whole-rock Rare Earth Element (REE) patterns for peridotites and pyroxenites are given in Table 3 and plotted in Fig. 6a (normalized to primitive mantle; McDonough & Sun, 1995). Dunites and harzburgites are strongly depleted in HREE (0·1–0·2 x PM) and one sample of dunite displays LREE enrichment, as do two samples of harzburgite. In contrast, lherzolites and wehrlite have HREE contents ranging from 0·4 to 1·4 x PM, and garnet pyroxenites have more enriched HREE contents, generally between 2·7 and 5·0 x PM. The three pyroxenite samples exhibit a relative depletion in LREE, whereas clinopyroxenite LM-38 is LREE enriched. The

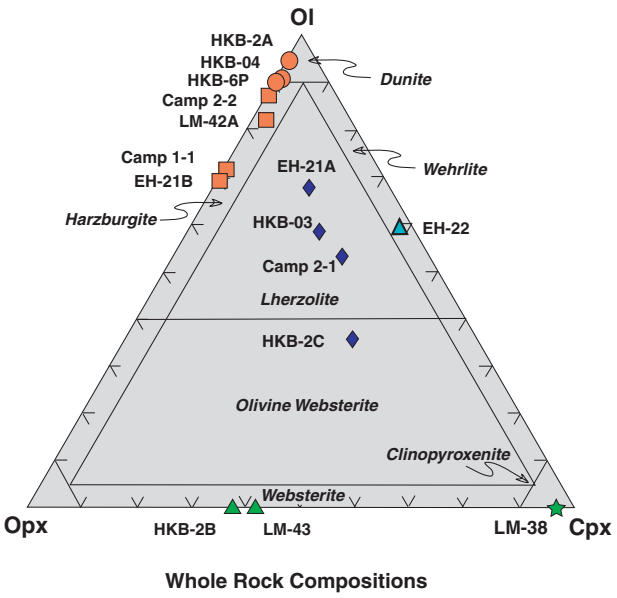

Fig. 3. Ternary diagram showing the relative proportions of initial olivine (ol), orthopyroxene (opx) and clinopyroxene (cpx) (garnet is understood to be present). The position on the diagram dictates the rock type identification listed in Table 1 and used throughout this study.

pyroxenites lack Eu anomalies, suggesting they crystallized initially as garnet- rather than plagioclase-pyroxenites. Extended trace element diagrams, normalized to primitive mantle, are plotted in Fig. 6b. They show positive anomalies for Ta and Pb and negative anomalies for Nb, Zr, Hf and Ti. Sr exhibits negative anomalies in some samples, but positive anomalies in others. Overall the pyroxenite patterns suggest a subduction signature.

Mineral chemistry

Major elements

The major element concentrations of major phases within the Tvaerdal peridotites and pyroxenites were measured by EMP at Macquarie University, The American Museum of Natural History and The University of Wisconsin-Madison. Table 4 presents average mineral concentrations based on point counts of adjacent minerals in polished thin sections for some samples and epoxy mounted grain separates for others, and averages of the flat portions of scans for selected samples. Complete mineral data are presented Supplementary Data Table S3a, including scans and averages for cores and rims. Additional mineral analyses for peridotite #6 are given in Augland *et al.* (2011). Primary minerals in the Tvaerdal ultramafic suite, like minerals in orogenic peridotite occurrences elsewhere, are magnesian, consisting of forsterite, enstatite, diopside and pyrope-rich garnet (Fig. 7a). Mg-numbers for forsterite (91·5–92·6), enstatite (89·3–93·0), diopside (90·7– 94·1), and garnet (76·9–82·0) largely overlap among the different rock types, except in clinopyroxenite, LM-38, where the Mg-numbers for diopside and garnet are 87·8 and 72·0, respectively. In contrast to the limited variation in Mg-numbers among the minerals, Cr-numbers in enstatite, diopside and garnet vary widely among rock types, being higher in peridotite than in pyroxenite. Cr-numbers for enstatite in peridotite and pyroxenite are 7·8–16·9 and 4·7, respectively; for diopside are 19·1–33·0 and 2·6–2·9; and for garnet are 6·5–14·0 and 0·5–1·5. FeO and Na_2O contents in clinopyroxene also vary widely, as illustrated in Fig. 7b. The concentrations of Cr_2O_3 in clinopyroxene are especially noteworthy, in view of the mixed assemblage model discussed subsequently. Clinopyroxenes in pyroxenites (HKB-2B and LM-38) have very low Cr concentrations, whereas clinopyroxenes in dunites and harzburgites (HKB-04, EH-21B and EH-22) have high Cr concentrations (Fig. 7b). Lherzolite and wehrlite clinopyroxenes have intermediate values and appear to define a single population, which contrasts with the two populations shown by garnet (see below).

Representative EMP scans across garnet, orthopyroxene, and clinopyroxene in pyroxenite HKB-2B and garnet in harzburgite EH-21B are illustrated in Fig. 8a and b. Most minerals are unzoned to weakly zoned for MgO and FeO, except for some garnets, which display a decrease in MgO and increase in FeO very close to the boundaries with kelyphite rims. Cr_2O_3 and CaO, however, are strongly zoned in garnets especially near the rims, as discussed further below. Orthopyroxenes in all scans, including lherzolite LM-42B (Fig. 8 a, c and d) show a characteristic increase in Al_2O_3 from core to rim (≈0·5% to ≈2·0%), reflecting re-equilibration during exhumation.

When garnet grains were separated from crushed rocks, it was discovered that different colours of garnet exist in four samples: dunite HKB-04 (violet and orange), lherzolite LM-42B (violet and pink), wehrlite EH-22 (violet, red and pink) and websterite HKB-02B (red and orange). These colour differences in some samples reflect core to rim variations in Cr_2O_3 content (e.g. HKB-2B); however, in other samples (e.g. LM-42B) they represent two populations of garnet containing different concentrations of Cr_2O_3, with higher amounts of Cr_2O_3 occurring in dark red or violet garnets and lower amounts of Cr_2O_3 in the lighter coloured garnets.

Lherzolite, sample LM–42B is particularly informative with respect to compositional variation in garnet and so its mineral chemistry was studied in more detail than in the other samples. It contains one set of violet, high–Cr garnet and a second set of pink, low–Cr garnet (Fig. 2g). Figure 9a illustrates the striking difference in Cr_2O_3 concentrations between the two sets. Also, in contrast to the garnets measured in most samples, the garnets in LM-42B are compositionally zoned (Fig. 9), although EMP traverses across grains do not reveal the entire, original compositional profiles because the grain margins were destroyed by subsequent growth of kelyphite rims. The Cr_2O_3 content in a high-Cr garnet (GM 1) decreases from ~6% in the core to ~5% in the inner rim, and abruptly to ~1·5% at the contact with kelyphite

Table 2: Peridotite and pyroxenite whole-rock major element chemistry, Tvaerdal complex, Liverpool Land

Sample	HKB-4	Camp 2-2		HKB-2A	HKB-6P	EH21A	LM42	Camp 1-1		EH21B	HKB-3	EH22	Camp2-1	HKB-2C	HKB-2B	LM 43	LM-38
Lith.	Dunite	Hrz		Dunite	Hrz	Lhrz	Pd	Hrz		Hrz	Lhrz	Lhrz	Whrl	Wbs	Cpxite	Wbstr	Cpxite
Oxides	Arranged in order of decreasing Mg#																
	n=2			n=2		n=2			n=2	n=2		n=2		n=2		n=2	n=2
Wt %																	
SiO2	43·0	42·7	41·8	42·8	47·8	43·4	45·5	45·3		45·7	44·8	46·6	47·1	48·1	46·6	45·2	
TiO2	0·012	0·023	0·020	0·020	0·098	0·024	0·0175	0·038		0·161	0·046	0·046	0·200	0·205	0·305	0·619	
Al2O3	0·709	2·09	0·768	1·19	4·97	1·80	0·811	1·31		6·07	6·10	3·12	8·91	10·2	12·4	13·2	
Cr2O3	0·335	0·256	0·347	0·184	0·419	0·243	0·203	0·300		1·035	0·542	0·207	0·354	0·366	0·102	0·129	
FeOt	7·01	7·08	7·45	7·36	6·04	7·36	7·35	7·32		6·09	7·30	7·83	6·89	6·88	8·73	10·6	
NiO	0·338	0·322	0·371	0·348	0·205	0·322	0·377	0·358		0·286	0·236	0·216	0·115	0·082	0·083	0·039	
MnO	0·096	0·112	0·071	0·109	0·174	0·111	0·055	0·091		0·171	0·169	0·151	0·205	0·227	0·239	0·255	
MgO	48·1	46·9	49·0	47·5	38·5	45·8	45·5	45·2		35·8	33·8	36·0	29·0	25·7	23·1	17·3	
CaO	0·396	0·548	0·093	0·470	1·44	0·975	0·137	0·080		4·19	6·72	5·63	7·00	8·16	7·60	11·8	
Na2O	0·001	0·016	0·000	0·031	0·246	0·004	0·000	0·000		0·505	0·282	0·135	0·096	0·084	0·818	0·511	
K2O	0·000	0·000	0·026	0·000	0·040	0·000	0·000	0·000		0·029	0·000	0·000	0·096	0·005	0·034	0·134	
P2O5	0·002	0·000	0·052	0·000	0·000	0·000	0·063	0·002		0·000	0·004	0·000	0·024	0·023	0·000	0·182	
Total	100·0	100·0	100·0	100·0	100·0	100·0	100·0	100·0		100·0	100·0	100·0	100·0	100·0	100·0	100·0	
Mg#	92·4	92·2	92·1	92·0	91·9	91·7	91·7	91·7		91·3	89·2	89·1	88·3	86·9	82·5	74·4	
Cr#	24·0	7·58	23·2	9·43	5·36	8·30	14·4	13·3		10·3	5·63	4·25	2·60	2·36	0·546	0·651	
Si	20·1	19·9	19·5	20·0	22·4	20·3	21·3	21·2		21·4	21·0	21·8	22·0	22·5	21·8	21·1	
Al	0·375	1·11	0·407	0·627	2·63	0·954	0·429	0·694		3·21	3·23	1·65	4·71	5·38	6·58	6·97	
Mg	29·0	28·3	29·6	28·7	23·2	27·6	27·4	27·2		21·6	20·4	21·7	17·5	15·5	13·9	10·4	
Ca	0·283	0·392	0·067	0·336	1·03	0·697	0·098	0·057		2·99	4·81	4·02	5·00	5·83	5·44	8·42	
Mg/Si	1·44	1·42	1·51	1·43	1·04	1·36	1·29	1·29		1·01	0·972	1·00	0·796	0·688	0·639	0·494	
Ca/Al	0·753	0·353	0·164	0·536	0·391	0·730	0·229	0·082		0·932	1·49	2·43	1·06	1·08	0·826	1·21	
Al/Si	0·019	0·056	0·021	0·031	0·118	0·047	0·020	0·033		0·150	0·154	0·076	0·214	0·239	0·302	0·330	

n = 2: average of two analyses (see Supplementary Data Appendix 2). All samples contain garnet or garnet relicts. Hrz, Harzburgite; Lhrz, Lherzolite; Whrl, Wherlite; Wbs, Websterite; Cpxite, Clinopyroxenite.

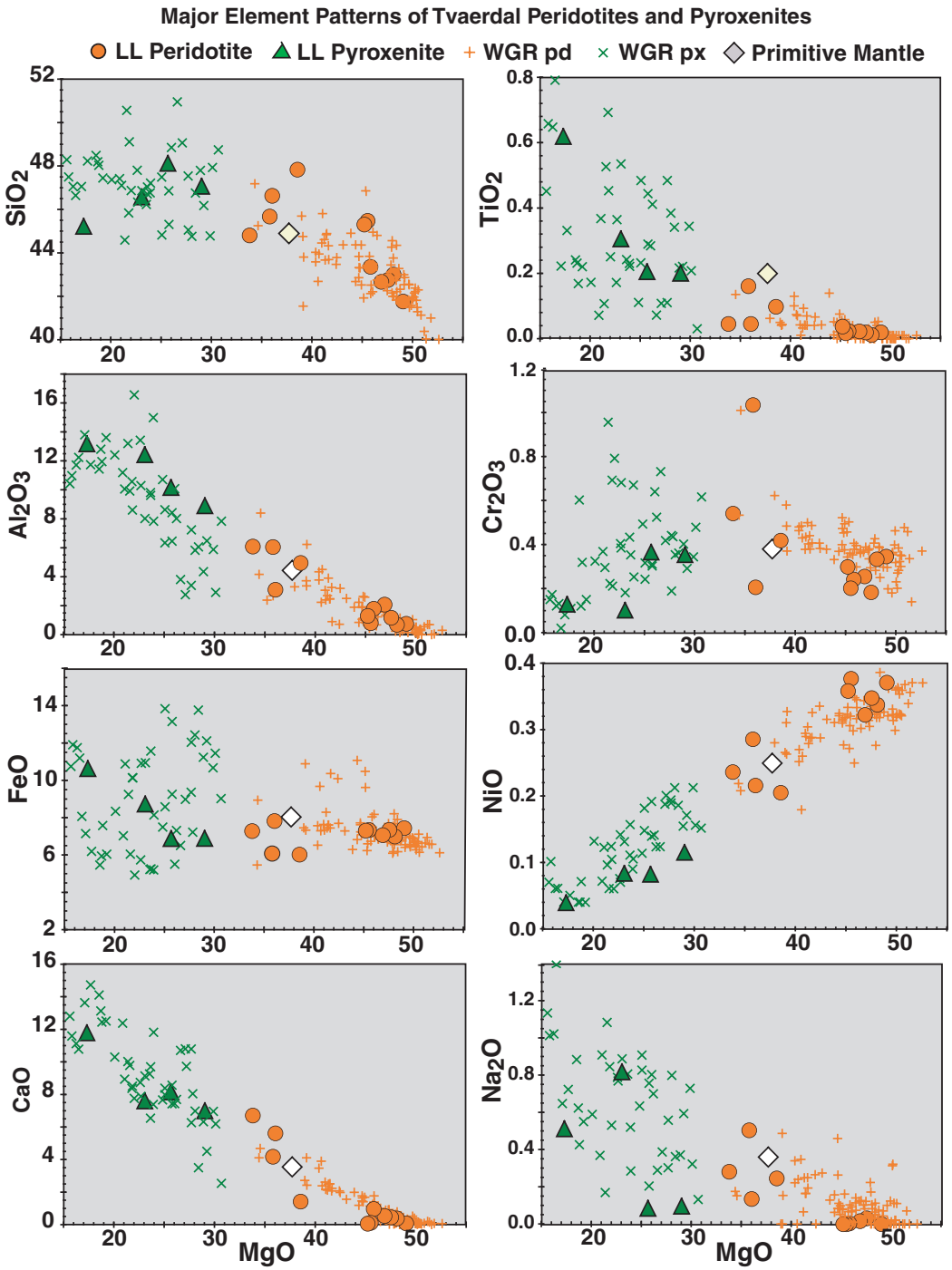

Fig. 4. Plots of major element concentrations of peridotites (large circles) and pyroxenites (large triangles) from the Tvaerdal Complex, Liverpool Land. The small symbols are analyses of peridotites (+) and pyroxenites (x) from the Western Gneiss Complex, Norway. WGC data are from Brueckner (HKB unpublished); Medaris (unpublished); Eskola, 1921; Mercy & O'Hara, 1965; Carswell, 1966 unpublished PhD dissertation, 1968a, 1968b, 1973, 1983; Carswell *et al.*, 2006; Lappin, 1974; Moore & Kvale, 1977; Al-Samman, 1985 unpublished PhD dissertation; Osland, 1997 and Beyer *et al.*, 2006. pd, peridotite; px, pyroxenite.

(Fig. 9a). In contrast, the Cr_2O_3 content in a low-Cr garnet (GM 2, Fig. 9a) increases from ~0·6% in the core to ~1·0% at the rim. Most other garnet grains in this sample show either a flat pattern or a core to rim increase in Cr_2O_3 and in several cases (e.g. HKB 1, GM 3 and HKB 3) this increase is asymmetric with an increase in Cr_2O_3 in one direction but no or only a very weak increase in the opposite direction. LM-42B may be different from most other studied samples in that some garnets are systematically zoned with respect to major elements (Fig. 9b). Most zoning is subtle, for example Cr-rich GM 1 shows a slight decrease from core to rim in pyrope and grossularite components and an increase in almandine component. The zoning of major elements in some

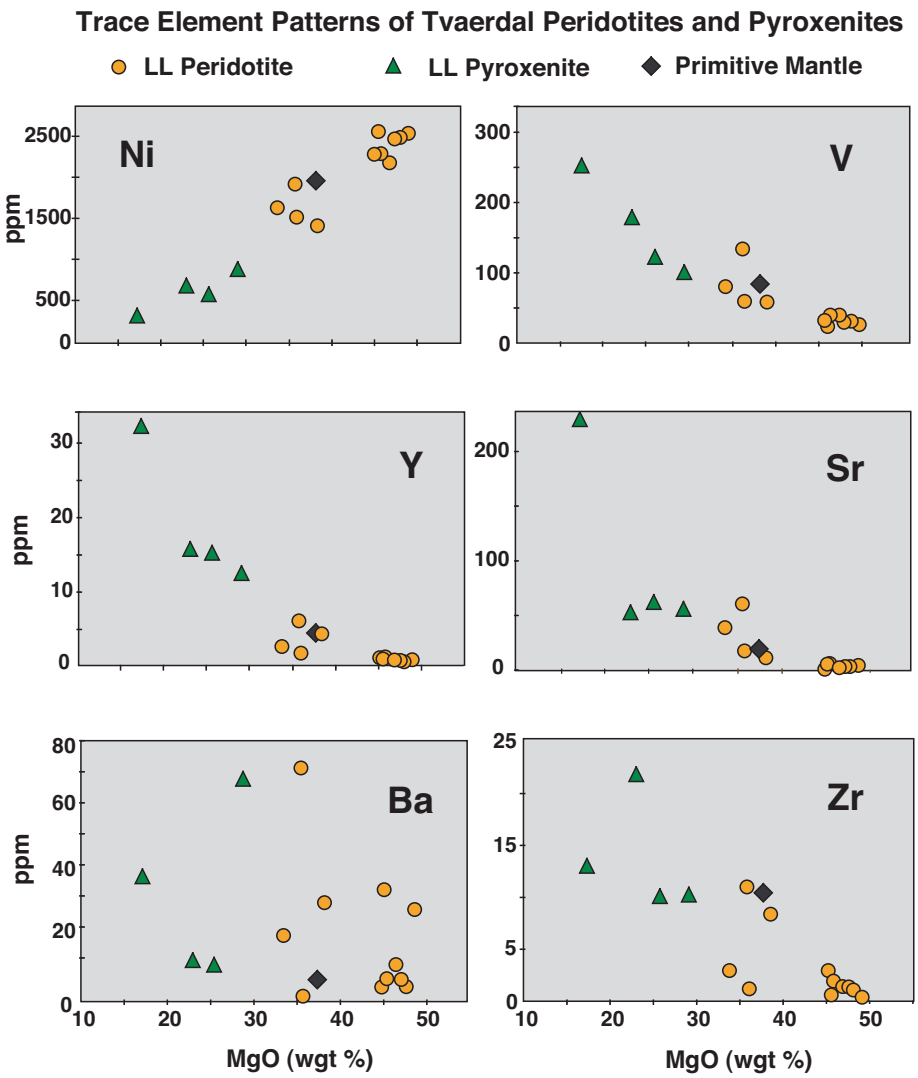

Fig 5. Plots of selected trace element concentrations from whole-rock Tvaerdal Complex peridotites, Liverpool Land.

low-Cr garnets differs from that in high-Cr garnet, with pyrope and grossularite slightly increasing from core to rim, and almandine decreasing. Other garnets show flat patterns. These patterns are enhanced by plotting the variation in Mg-number across the garnet (Fig. 9b), where it can be seen that only the high-Cr garnet GM 1 shows a marked decrease in Mg-number from core to rim. The rest of the garnets show flat patterns or only minor variation. Nevertheless, the figure does illustrate that there is significant variation in Mg-number between grains.

Amphibole is localized in and around the kelyphite rims and consists of pargasite in harzburgite, lherzolite, and wehrlite, and tschermakite in websterite. The spinel associated with garnet shows a large range in composition between (Fig. 10a) and within samples (Fig. 10b). Spinels in LM-42B within garnet and orthopyroxene, and the olivine-rich matrix are relatively Cr-rich, whereas those within the kelyphite reaction rims are more enriched in Al (Fig. 10b), although there is a large overlap in compositions between the domains.

Trace elements (REE)

Selected peridotite minerals were analysed for trace elements by LA-ICP-MS and their REE abundances relative to chondritic mantle are plotted in Fig. 11a (clinopyroxene) and 11b (garnet). REE patterns for each separate sample are plotted in Supplementary Data Table S3B. Clinopyroxenes from most samples show the classic 'hooked' pattern, with positive slopes for the Light Rare Earth Elements (LREE) followed by negative slopes for the Middle Rare Earth Elements (MREE) and Heavy Rare Earth Elements (HREE). In contrast, the clinopyroxene REE pattern for wehrlite EH-22 displays a negative slope throughout.

REE patterns for garnet display LREE depletion, which is a common feature in garnet from orogenic peridotites. Garnets from four rock samples have comparable MREE to HREE patterns (i.e. Sm to Lu), which are either flat or gently sloping. However, slopes for the LREE vary among the four samples, depending on rock type and the colour of garnet. The LREE slope is steep for a single garnet separate from lherzolite LM–42B and

Table 3: Peridotite and pyroxenite whole-rock trace element chemistry (in ppm), Tvaerdal Complex, Liverpool Land

Sample	HKB-4	Camp 2-2	HKB-2A	HKB-6P	EH-21A	LM42	Camp 1-1	EH-21B	HKB-3	EH-22	Camp 2-1	HKB2C	HKB2B	LM 43	LM38
Lithology	Dunite	Hrz	Dun	Hrz	Lhrz	Pd	Hrz	Hrz	Lhrz	Hhrz	Whrl	Wbstr	Cpxite	Wbstr	Cpxite
Li	2·18	1·28	2·50	0·961	6·26	0·980	4·67	4·38	5·2	2·51		6·94	4·71	3·29	7·71
Be	0·007		0·047		0·047			0·026	0·145	0·016		0·308	0·355		0·727
Sc	5·97	8·64	3·75	7·27	13·0	9·16	6·65	5·98	30	20·1	22·3	30·13	34·9	36·4	61·4
Ti	98·7	172	103	188	528	224	88·6	232	901	308	329	1145	1307	1846	3564
V	30·2	39·5	25·97	30·0	57·9	40·0	24·8	32·6	133	80·4	59·0	97·8	119	174	248
Cr	1954	1501	1468	1130	2387	1501	1192	1361	5914	2663	1266	1787	1789	689	531
Mn	736	701	479	761	1221	745	378	670	1200	1268	993	1528	1810	1817	2008
Co	109	91·5	112	102	68·3	107	107	95·4	81	87·9	95·5	63·3	44·09	95·2	44·4
Ni	2478	2172	2520	2454	1402	2285	2542	2274	1909	1618	1520	864	557	649	289
Cu	5·91	12·8	2·45	7·11	17·4	12·7	3·63	7·87	97·7	41·6	5·86	3·9	3·52	11·7	11·3
Zn	37·6	35·7	57·6	41·5	31·3	40·8	48·6	36·3	34·8	25·8	35·1	24·9	17·1	19·8	17·7
Ga	0·548	1·23	0·712	0·89	3·53	1·29	0·74	1·19	3·38	3·62	2·07	5·60	6·10	8·64	7·89
Rb	0·073	0·058	0·686	0·089	1·79	0·098	0·240	0·11	1·41	0·11	0·049	2·67	0·53	0·713	7·67
Sr	3·33	3·06	4·35	4·00	12·2	6·40	5·61	1·10	60·6	39·8	18·0	53·9	60·17	50·8	227
Y	0·460	0·741	0·674	0·687	4·10	0·973	0·750	0·92	6·0	2·51	1·64	12·0	14·8	15·4	31·9
Zr	1·04	1·40	0·420	1·36	8·28	2·00	0·632	2·98	10·9	2·97	1·22	9·93	9·81	21·5	12·8
Nb	0·057	0·092	0·169	0·035	0·062	0·089	0·210	0·042	0·36	0·07	0·100	0·72	0·62	0·379	1·00
Mo	0·107	0·355	0·067	0·246	0·150	0·132	0·076	0·186	0·16	0·17	0·147	0·33	0·16	0·22	0·30
Cd	0·008	0·013	0·013	0·012	0·026	0·015	0·008	0·011	0·07	0·03	0·027	0·05	0·06	0·076	0·09
Cs	0·030	0·026	0·063	0·011	1·7	0·017	0·202	0·044	0·56	0·01	0·054	0·60	0·38	0·14	0·51
Ba	4·48	11·2	27·9	6·61	30·0	7·03	33·8	4·11	71·0	20·0	1·45	67·0	10·5	11·8	37·5
La	0·079	0·242	0·450	0·092	0·208	0·139	0·521	0·190	1·37	0·66	0·359	0·61	0·56	0·68	8·97
Ce	0·170	0·634	1·36	0·239	0·710	0·377	1·42	0·416	4·66	1·06	0·669	2·43	2·44	2·21	26·2
Pr	0·028	0·093	0·192	0·042	0·147	0·064	0·187	0·077	0·93	0·13	0·083	0·46	0·49	0·41	3·62
Nd	0·133	0·408	0·820	0·206	0·949	0·327	0·779	0·451	4·96	0·54	0·352	2·56	2·78	2·37	16·5
Sm	0·056	0·100	0·152	0·070	0·380	0·116	0·178	0·156	0·80	0·15	0·126	1·09	1·26	0·87	4·66
Eu	0·023	0·037	0·041	0·026	0·128	0·043	0·062	0·045	0·23	0·06	0·047	0·47	0·53	0·34	1·36
Gd	0·071	0·119	0·140	0·095	0·499	0·147	0·196	0·167	0·81	0·23	0·201	1·47	1·77	1·52	5·76
Tb	0·012	0·020	0·020	0·016	0·087	0·024	0·030	0·025	0·13	0·04	0·038	0·25	0·31	0·298	1·01
Dy	0·072	0·127	0·110	0·105	0·581	0·156	0·154	0·146	0·88	0·35	0·269	1·68	2·10	2·18	5·56
Ho	0·015	0·028	0·022	0·024	0·131	0·035	0·026	0·030	0·21	0·09	0·062	0·39	0·49	0·52	1·02
Er	0·042	0·082	0·058	0·070	0·384	0·099	0·060	0·083	0·63	0·27	0·181	1·15	1·46	1·54	2·60
Yb	0·0447	0·087	0·053	0·076	0·387	0·093	0·046	0·078	0·61	0·30	0·185	1·16	1·48	1·53	2·23
Lu	0·0073	0·014	0·0083	0·012	0·061	0·015	0·007	0·013	0·10	0·05	0·027	0·18	0·23	0·24	0·34
Hf	0·0223	0·040	0·0052	0·036	0·212	0·054	0·011	0·086	0·39	0·10	0·049	0·22	0·21	0·664	0·30
Ta	0·278	0·030	0·0051	0·025	0·194	0·107	0·026	0·014	0·25	0·22	0·178	1·18	0·04	0·817	0·08
Pb		2·41		1·39		2·08	1·42				3·22			2·66	
Th	0·0136	0·039	0·020	0·007	0·008	0·012	0·035	0·016	0·03	0·04	0·043	0·05	0·05	0·060	0·61
U	0·0049	0·009	0·0166	0·003	0·002	0·009	0·006	0·307	0·01	0·01	0·006	0·01	0·01	0·028	0·16

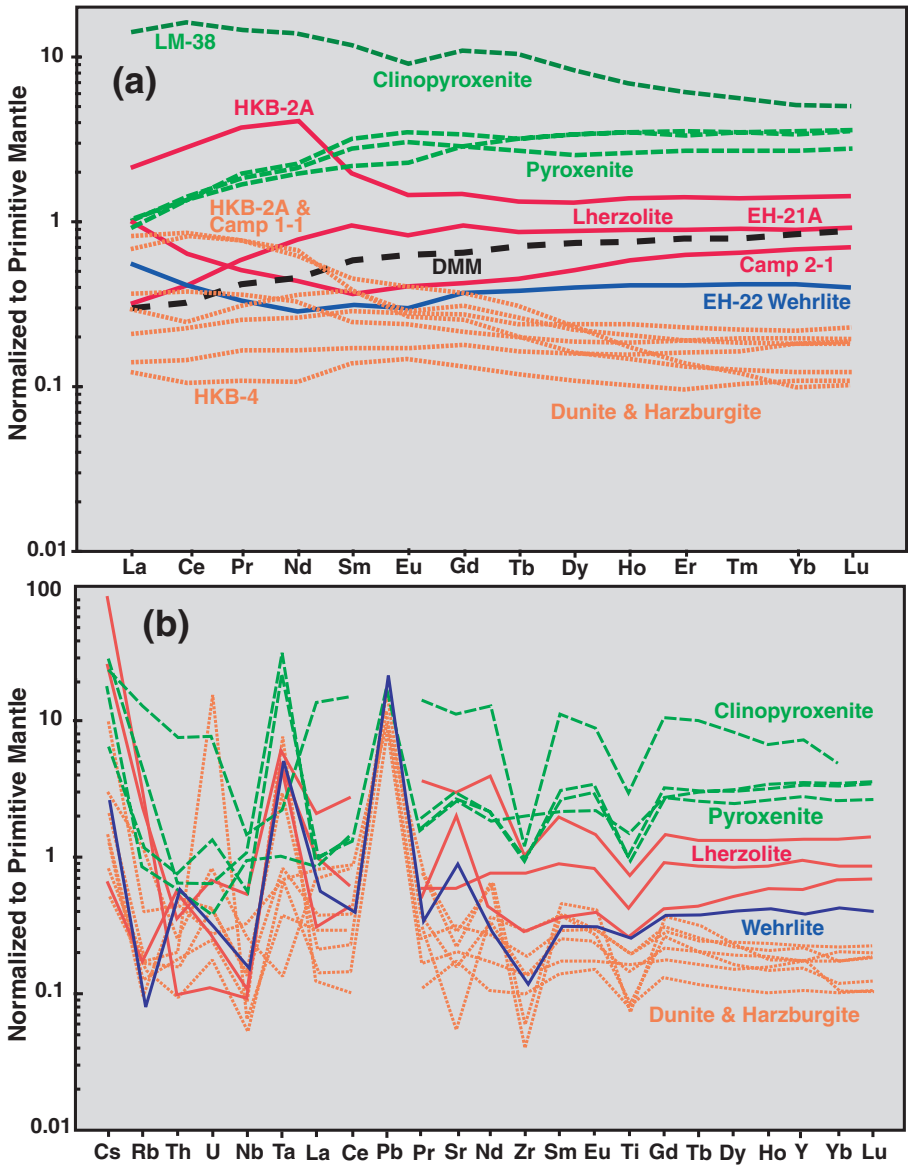

Fig. 6. (a) Rare Earth Element and (b) Extended trace element patterns of Tvaerdal ultramafic rocks, normalized to Primitive Mantle (McDonough & Sun, 1995).

comparably steep for violet, red and orange garnets from dunite HKB–04 (notwithstanding the 'spike' in Ce for one of the violet garnet separates). In contrast, in wehrlite EH–22, the LREE slope for violet garnet is steep, whereas the LREE slope for red and orange garnets is flat. Interestingly, this wehrlite sample is the only one among the four that shows whole-rock LREE enrichment. The LREE slope for garnet from olivine websterite HKB–2C is intermediate between those of the other samples. Nevertheless, the flat or even slightly negative slopes for the LREE shown by some garnets suggest LREE enrichment.

P–T calculations

A combination of geothermobarometers (Supplementary Data Table S3C) was utilized to estimate *P–T* conditions for the LL ultramafic suite, including Fe–Mg exchange geothermometers for olivine and garnet (Wu & Zhao, 2007) and orthopyroxene and garnet (Harley, 1984), and the Al-in-opx geobarometer (Nickel & Green, 1985). Application of these methods to the core compositions of adjacent minerals (Fig. 12) yields *P–T* estimates of 36·9 kbar/804°C for dunite (HKB–04), 31·8 kbar/848°C for harzburgite (EH21B) and 24·4 kbar/818°C for lherzolite (HKB–03). Websterite (HKB-2B) yields 32·9 kbar/864°C, which is comparable in temperature to the peridotites, but lower in pressure. Wehrlite EH-22 and clinopyroxenite LM-38 did not give reliable pressure estimates, but an assumed pressure of 30 kbar yielded temperatures (≈900°C and ≈830°C, respectively) consistent with the other measurements. These values yield an overall estimate of 30·5 kbar/801°C, which lies just below the very high maximum average *P–T* (35·1 kbar/877°C) calculated for an external orthopyroxene-

Table 4: Mineral major element chemistry, Tvaerdal Complex, Liverpool Land

		SiO_2	TiO_2	Al_2O_3	Cr_2O_3	FeO	MnO	MgO	CaO	Na_2O	K2O	NiO	Total	Mg#	Cr#	Ca#
LM-42B	Lherz															
ol	scan (20)	40·5	0·010	0·001	0·011	8·26	0·119	50·1	0·008	0·008		0·454	99·4	91·5	86·9	
opx	scan (90)	56·6	0·044	0·962	0·140	5·64	0·117	35·3	0·220	0·024		0·089	99·1	91·8	8·89	
cpx	scan (25)	53·2	0·108	2·23	0·845	2·94	0·065	16·1	21·41	1·46		0·051	98·3	90·7	20·3	46·5
hi-Cr grt	scan (109)	40·9	0·070	20·0	4·12	9·95	0·501	19·1	4·75	0·029		0·011	99·4	77·3	12·2	12·2
lo-Cr grt	scan (200)	41·7	0·033	23·2	0·355	9·01	0·432	20·9	3·73	0·019		0·014	99·4	80·5	1·02	9·37
LM-38	Cpxite															
cpx	disc (2)	54·6	0·056	1·49	0·067	4·03	0·057	16·3	22·40	1·28	0·011	0·068	100·4	87·8	2·93	46·5
amph	disc(1)	43·5	0·055	17·1	0·212	13·2	0·421	26·8	0·579	0·017	0·009	0·036	101·9	78·3	0·83	1·20
grt	disc (2)	42·2	0·076	23·3	0·183	12·9	0·463	18·6	4·58	0·021	0·009	0·017	81·8	72·0	0·53	11·3
HKB-2B	Websterite															
ol	no ol															
opx	scan (6)	56·5	0·071	1·55	0·115	6·09	0·122	34·3	0·267	0·010	0·009	0·093	99·09	90·9	4·74	
cpx	scan (7)	53·5	0·115	1·41	0·055	2·30	0·063	17·3	24·41	0·282	0·003	0·042	99·41	93·0	2·54	48·6
amph	spot (1)	46·5	0·395	14·8	0·324	3·27	0·060	17·7	12·95	1·27	0·029	0·033	97·45	90·6	1·44	32·2
grt	scan (32)	41·4	0·069	23·3	0·43	10·3	0·513	19·2	4·99	0·005	0·006	0·009	100·2	76·9	1·23	0·13
red grt	spot (1)	42·5	0·070	23·7	0·577	9·71	0·420	19·8	5·11	0·002	0·006	0·037	102·0	78·4	1·61	12·7
orng grt	spot (1)	42·6	0·077	24·2	0·086	9·92	0·427	20·3	4·32	0·010	0·009	0·000	101·9	78·5	0·24	10·7
HKB-3	Lherz															
ol	spot (3)	41·8	0·008	0·005	0·009	7·94	0·169	50·5	0·017	0·004	0·010	0·409	100·8	91·9	56·4	
opx	disc (2)	57·5	0·061	1·57	0·263	5·40	0·178	35·6	0·269	0·01	0·014	0·061	100·9	92·2	10·1	
cpx	spot (2)	54·6	0·134	2·76	1·48	1·84	0·068	16·3	22·51	1·34	0·009	0·022	101·1	94·1	26·4	48·2
grt	disc (1)	42·3	0·133	22·7	2·38	8·85	0·447	20·4	4·35	0·003	0·006	0·003	101·6	80·5	6·55	11·0
amph	disc (2)	45·3	0·436	12·7	1·80	3·20	0·020	18·6	12·53	2·55	0·177	0·099	97·4	91·2	8·72	30·7
HKB-4	Dunite															
ol	spot (3)	41·6	0·006	0·006	0·010	7·27	0·116	51·0	0·014	0·019	0·011	0·396	100·5	92·6	51·5	
opx	disc (2)	58·6	0·027	0·552	0·167	4·87	0·110	36·2	0·204	0·026	0·015	0·104	100·9	93·0	16·8	
cpx	spot (3)	54·7	0·049	1·74	1·28	2·02	0·054	16·4	22·46	1·49	0·000	0·060	100·3	93·6	33·0	47·9
violet grt	disc (2)	41·6	0·086	20·6	4·95	9·08	0·463	19·4	5·33	0·015	0·000	0·000	101·5	79·2	13·9	13·5
orng grt	disc (2)	42·6	0·142	23·1	1·59	9·34	0·434	20·7	4·20	0·029	0·000	0·012	102·1	79·8	4·41	10·4
EH-21B	Harzburg															
ol	no analyses															
opx	scan (14)	57·8	0·053	0·956	0·121	5·02	0·108	35·6	0·187	0·009	0·003	0·087	99·94	92·7	7·82	
cpx	spot (3)	54·3	0·193	3·51	1·54	1·89	0·037	15·3	20·97	2·36	0·004	0·026	100·2	93·5	22·7	48·0
amph	spot (2)	44·0	0·746	14·8	1·18	3·54	0·027	17·9	11·83	3·23	0·468	0·133	97·82	90·0	5·07	29·9
grt	scan (32)	42·6	0·060	23·7	1·05	8·44	0·405	21·6	3·50	0·010	0·006	0·009	101·3	82·0	2·89	8·71
grt	spot (1)	42·4	0·179	22·1	3·05	8·97	0·48	20·6	4·03	0·025	0·005	0·004	101·8	80·3	8·47	10·1
grt	spot (1)	42·4	0·097	21·2	4·38	8·74	0·47	21·2	3·39	0·001	0·000	0·000	102·0	81·2	12·2	8·52
EH-22	Wehrlite															
ol	spot (3)	41·0	0·002	0·004	0·010	9·89	0·18	48·9	0·011	0·002	0·001	0·41	100·4	89·8	60·2	
opx	spot 1	56·9	0·006	2·63	0·092	7·24	0·206	33·8	0·297	0·009	0·002	0·12	101·3	89·3	2·28	
cpx	scan (10)	54·2	0·067	1·69	0·669	2·32	0·05	17·2	22·9	0·88	0·006	0·04	100·1	93·0	21·0	47·2
amph	spot (7)	45·4	0·302	13·3	1·43	4·27	0·06	18·3	12·2	2·81	0·079	0·10	98·2	88·4	6·72	29·7
grt	scans (21)	42·2	0·062	22·9	1·57	9·98	0·48	19·6	4·87	0·010	0·003	0·01	101·6	77·8	4·41	12·2
violet grt	disc (1)	42·5	0·072	21·9	3·54	8·53	0·480	20·2	4·96	0·008	0·006	0·000	102·2	80·8	9·77	12·5
red Grt	disc (1)	42·7	0·102	23·3	1·59	9·38	0·503	20·2	4·41	0·015	0·003	0·000	102·2	79·3	4·39	11·1
pink grt	disc (1)	42·3	0·082	23·4	1·39	9·32	0·457	20·2	4·48	0·000	0·000	0·018	101·7	79·5	3·82	11·2

Spinel compositions vary too much for averaging. See Appendix 3. Mineral abbreviations as in Table 1.
Parenthesis, number of analyses; scan, grain traverse; spot, single analysis of grain thin section.
disc, single grains mounted and polished in epoxy and analysed.

bearing eclogite (EH-15B) in the nearby gneisses (Brueckner *et al.*, 2016).

Two measurements, from two different laboratories, of high-Cr garnets from LM-42B yielded similar values (29·7 kbar/784°C and 32·1 kbar/789°C). These pressures are similar to the pressures defined by the ultramafic samples discussed above, but the temperatures are lower. A low-Cr garnet, when combined with the same forsterite and enstatite compositions as the high-Cr garnet, yields the same *P–T* (38·6 kbar/897°C) as the orthopyroxene eclogite. However, if this sample contains mixed peridotite/pyroxenite assemblages, as we discuss further below, all calculations from LM-42B should be treated with caution.

Application of the same geothermobarometers to rim compositions of minerals yields pressures of 15–25 kbar and temperatures of 750–800°C (Fig. 12). The original rims of the garnet were replaced by kelyphite, so these *P–T* values do not represent the values of the original rims, which were probably lower than the core values. Regardless, the present *P–T* rim values indicate that the initial stage of decompression was largely isothermal, similar to the pattern shown by the external eclogite.

The core *P–T* values of most samples fall more or less along the retrograde path defined by the external eclogite (Fig. 12). We suggest that these samples re-equilibrated to varying degrees during post-Scandian

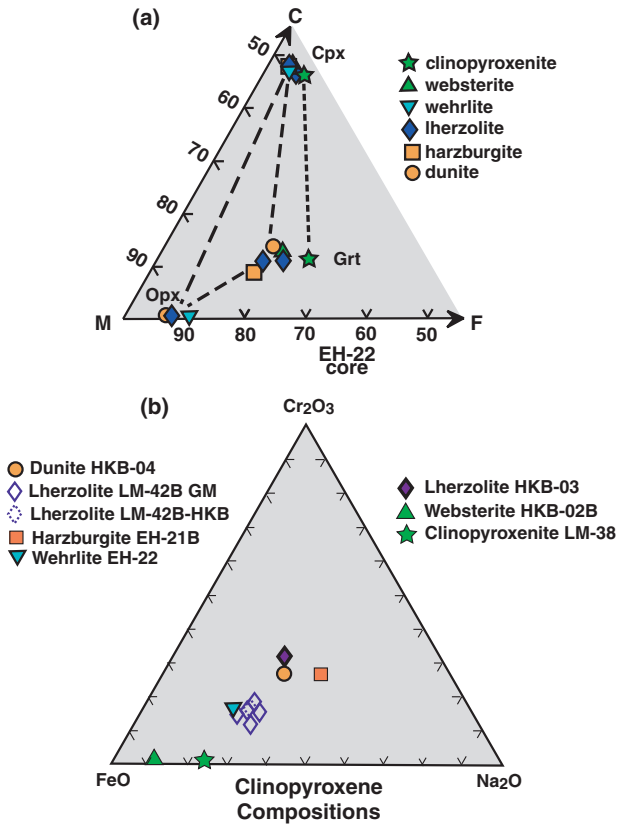

Fig. 7. (a) Representative compositions of orthopyroxene (opx), clinopyroxene (cpx) and garnet (grt) in the system Ca–Mg–Fe (C–M–F), identified by rock type. (b) Representative compositions of clinopyroxenes in the Cr_2O_3–FeO–NaO system. Note the positions of LM-42B and EH-22 clinopyroxenes with Cr_2O_3 contents intermediate between clinopyroxenes from dunites and harzburgites and clinopyroxenes from pyroxenites. These intermediate compositions may be the result of re-equilibration between the two end-members (see discussion for further details).

retrogression. The garnets from HKB-04 and high-Cr LM-42B fall off this trend and plot at lower temperatures. Both garnets are high-Cr garnets, which are believed to have formed during a pre-Scandian event (see discussion below). Their *P–T* values may reflect conditions during this older metamorphism. Alternatively the standard geothermobarometers may not apply accurately to garnets with high Cr-contents or none of the garnets were in equilibrium with the adjacent minerals as a result of mechanical mixing.

Geochronology

Mineral separates from websterites HKB-2B and LM-43, wehrlite EH-22 (Table 1) and pyroxenite LEA 08–04 were analysed for their Sm, Nd and Sr concentrations and Sr and Nd isotope compositions (Table 5, Fig. 13). Obtaining reliable ages was complicated by the fact that all four samples contain garnet separates with mixtures of different colours, including violet, dark red, pink, orange and pale red. These colour variations were initially interpreted as reflecting core to rim chemical variations, which is seemingly confirmed by Cr-profiles across grains (Figs 8 and 9). Because the REE are, like Cr, trivalent, it is likely that REE concentrations vary from core to rim as well, precluding the possibility that a given sample would yield a single recrystallization age. Nevertheless, garnet grains were separated by colour under a binocular microscope with the hope of obtaining at least some time constraints on core vs rim formation. Due to the nature and amount of separated garnet, it was only possible to divide garnet separates into two fractions and it proved difficult to obtain absolutely pure end-member separates.

Parts of websterite sample HKB-2B display clean granoblastic fabrics with little evidence of fracturing (Fig. 2l). Nevertheless, repeated analyses of garnets from this websterite plot as scattered points and fail to show a consistent relationship between age and garnet colour (Fig. 13a). Despite this scatter, the data give interpretable results in that the garnet that generates the steepest slope gives a clinopyroxene–whole-rock–garnet isochron age of 432 ± 5 Ma (2 σ, MSWD = 0·003) whereas the garnet that generates the shallowest slope gives a near-isochron age of 409 ± 6 Ma (MSWD = 1·3). Thus, despite the scatter, the 'ages' from this websterite, indicate that garnet formation in the pyroxenites probably began during the earliest stages of the Scandian Orogeny (≈430 Ma Sm–Nd isochron ages were obtained from garnet pyroxenites of the WGC by Spengler *et al.*, 2009). The 409 Ma age of the 'youngest' garnet is within error or very close to the Scandian ages obtained from Tvaerdal eclogites (Brueckner *et al.*, 2016), suggesting a shared history. This conclusion is supported by the results from pyroxenite LM-43 (Fig. 13b) from which several garnet fractions were analysed along with clinopyroxene, amphibole and whole-rock. The different fractions are slightly scattered, but cluster around an age of 399 ± 18 Ma (MSWD = 18). Some of this scatter is attributable to the different colours of the garnet fractions (the exact colour of grt2 was not noted). The most precise age of 403·6 ± 7·5 (MSWD = 0·56) is defined by grt2 and the lighter coloured ('pale') garnet fraction, whereas the darker red garnet defines a younger age (387·8 ± 7·5 Ma; MSWD = 0·84). Despite the lack of a true isochron age, the results from both pyroxenite samples are consistent with pyroxenite HP/UHP equilibration during the Scandian Orogeny.

The data from the garnets in wehrlite EH-22 (Fig. 13c) and peridotite LEA 08–04 (Fig. 13d) complicate this relatively straightforward picture. As in websterite HKB-2B, the darker garnet fractions in both samples collectively define steeper best-fit lines than those defined by pale garnets. The clinopyroxene–whole-rock–garnet best-fit lines with the steepest slopes generate apparent ages of 808 ± 48 Ma in EH-22 and 729 ± 18 Ma in LEA 08–04. These ages do not match pre-Scandian orogenic events recorded in the associated gneisses (i.e. the 1·6 Ga Labradoran orogeny and the 1·0 Ga Grenville orogeny) and should be considered minimum estimates that were partially re-set during Scandian crystallization.

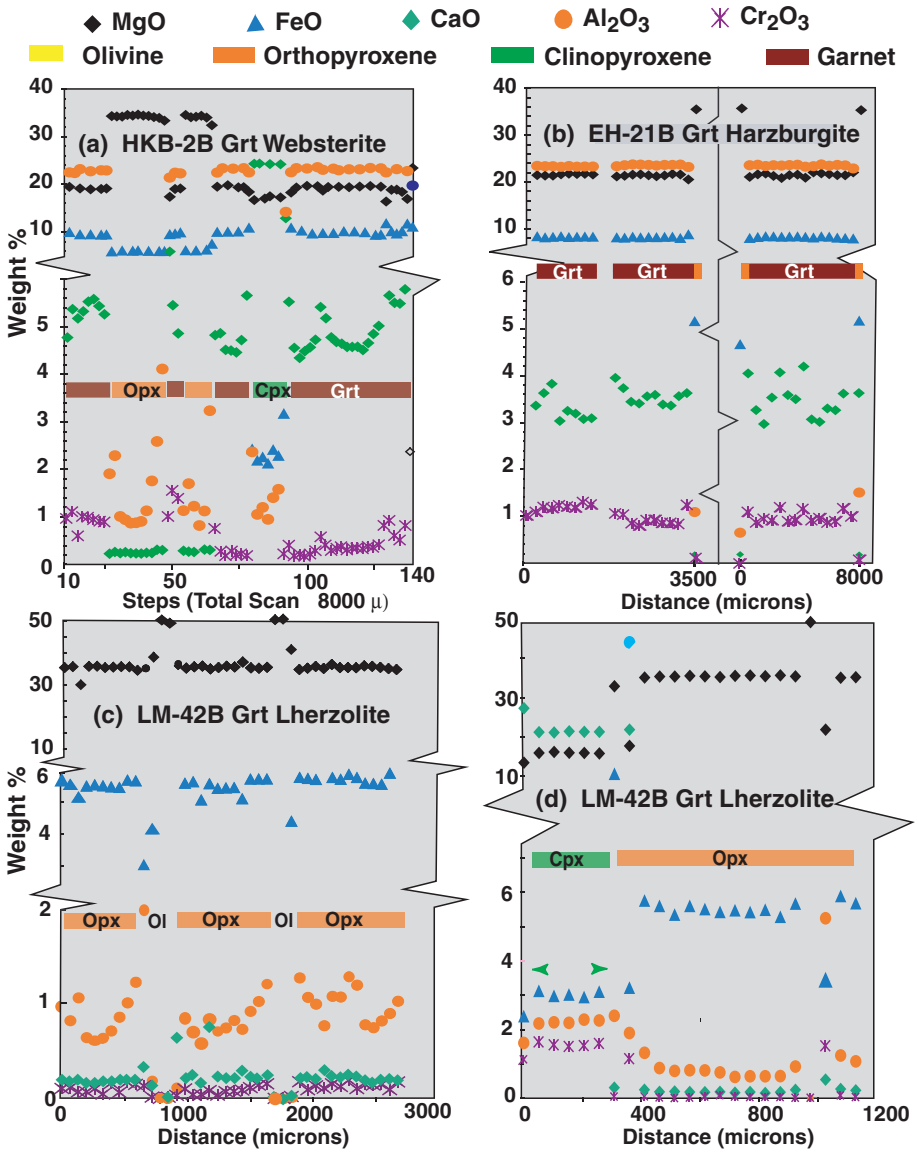

Fig. 8. Rim-to-rim EMP scans for major oxide concentrations for selected minerals from Tvaerdal peridotites and pyroxenites. (a) Typical scan across orthopyroxene, clinopyroxene and garnet in pyroxenite HKB-2B, showing flat patterns for most elements except for Al in orthopyroxene and Cr and Ca in garnet (Cr concentrations deleted for clinopyroxene and orthopyroxene for clarity). Also note different Cr contents for different garnets. (b) Scans across garnets in EH-21B. Again, note the flat patterns for most elements except Cr and Ca. (c, d). Scans across olivine, orthopyroxene and clinopyroxene in lherzolite LM-42B. Major elements show flat patterns except for Al_2O_3 in orthopyroxene in contact with olivine (c) and clinopyroxene (d). Some measurements have been deleted for clarity where the data are too crowded. Data for these scans are given in Supplementary Data Table S3a.

The pale garnets with the shallowest slopes give apparent ages of 647 ± 13 Ma in EH-22 and 384 ± 32 Ma in LEA 08–04. The pre-Caledonian 647 Ma age in EH-22 is considered a maximum age of the younger of two garnet generations, which proved impossible to completely separate from the older darker garnets. The two pale garnets in LEA 08–04, however, appear to have been successfully separated from older garnets. They give Scandian ages of 384 ± 32 Ma and 425 ± 15 Ma (not plotted) when regressed separately with two clinopyroxenes and the whole-rock. The apparent age calculated using both pale garnets (414 ± 44 Ma) is not an isochron (MSWD = 14), but together the apparent ages indicate that the pale garnets in this sample formed during the Scandian orogeny, consistent with the results from the garnet pyroxenites.

Sr–Nd isotope variations

$^{87}Sr/^{86}Sr$ and $^{143}Nd/^{144}Nd$ values of clinopyroxenes and amphiboles from nine Tvaerdal garnet peridotites and pyroxenites (Table 5) and two Tvaerdal eclogites (Brueckner *et al.*, 2016) are plotted in Fig. 14, where they are compared with the isotopic compositions of clinopyroxenes from WGC peridotites, pyroxenites (Brueckner *et al.*, 2010) and eclogites (Brueckner,

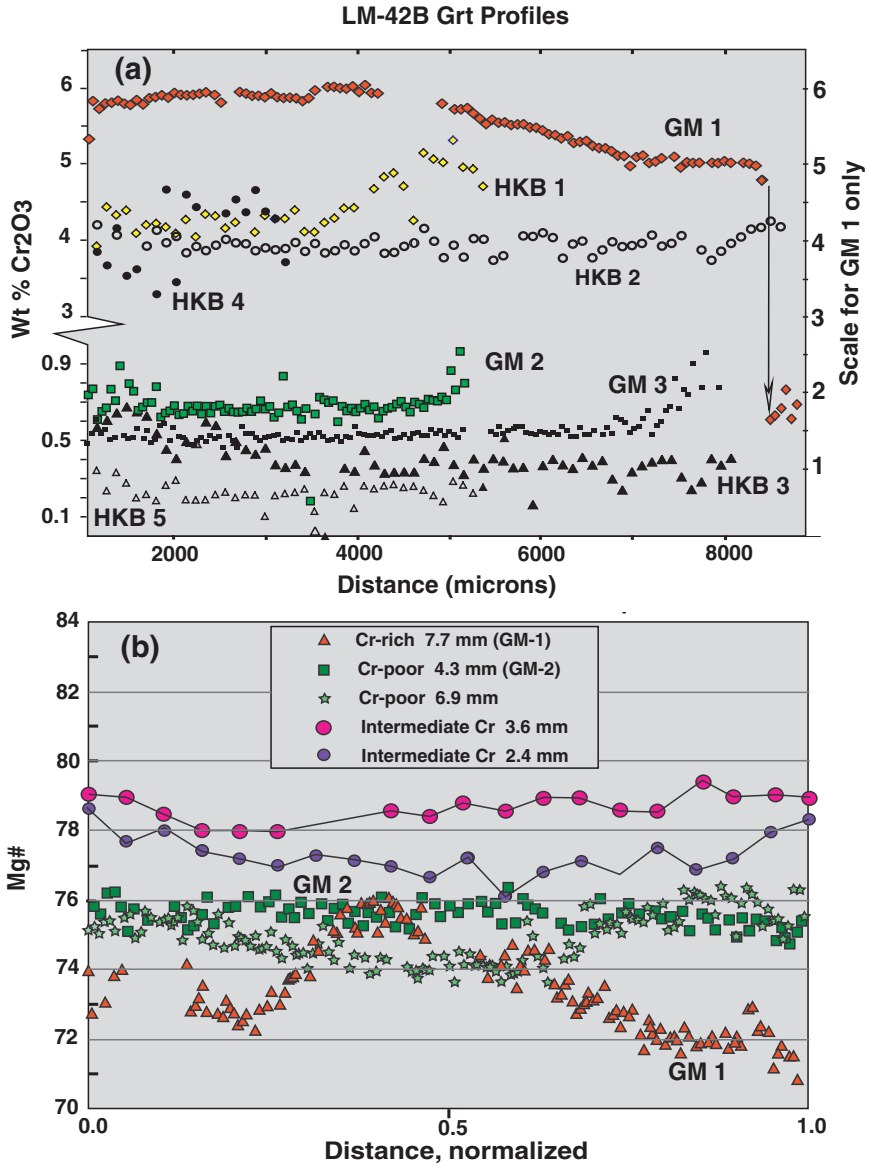

Fig. 9. (a) Rim to rim Cr_2O_3 traverses across garnets within lherzolite LM-42B. Note large gap in Cr_2O_3 concentrations between Cr-rich and Cr-poor garnets. Grt 1 is the only garnet scanned in LM-42B that shows a decrease for core to rim. The remaining garnets show increasing Cr concentrations towards the rims, many of which are asymmetric, suggesting that they are fractured grains. (b) Rim-to-rim scans showing changes in Mg-number across garnet grains. The use of Mg-number and a restricted scale (70–84) enhances the relatively slight variations across the grains, which nevertheless are flat for many grains (GM 2) except for the Cr-rich garnet GM 2. The significant variations in Mg content between grains also suggests that the garnets are fragments of larger grains that had significant gradients in Mg concentration. HKB and GM refer to the analysts.

unpublished data). Most WGC ultramafic clinopyroxenes define a steep array with variable $^{143}Nd/^{144}Nd$ and restricted, low $^{87}Sr/^{86}Sr$. Such an array implies that most WGC clinopyroxenes formed or equilibrated within the mantle (Brueckner *et al.*, 2010). In contrast, clinopyroxenes from the Tvaerdal peridotites and pyroxenites plot along the trend defined by WGC eclogites, though not to the very high $^{87}Sr/^{86}Sr$ ratios in some enriched WGC eclogites. This trend suggests that ultramafic Tvaerdal clinopyroxenes with initial mantle values (high $^{143}Nd/^{144}Nd$, low $^{87}Sr/^{86}Sr$) equilibrated to varying degrees with high $^{87}Sr/^{86}Sr$, low $^{143}Nd/^{144}Nd$ fluids derived either from a subducting slab or from the surrounding crustal rocks.

Re–Os

The results of a LA-ICP-MS Re–Os study of sulfides from the Tvaerdal peridotite are listed in Table 6 (the complete data set is included in Supplementary Data File 4). Only four samples, EH-21 and 22, HKB-3 and Camp 2–1 contained sulfides with measurable Os and relatively low Re concentrations. Figure 15a is a Re–Os isochron diagram that plots all measured sulfides with

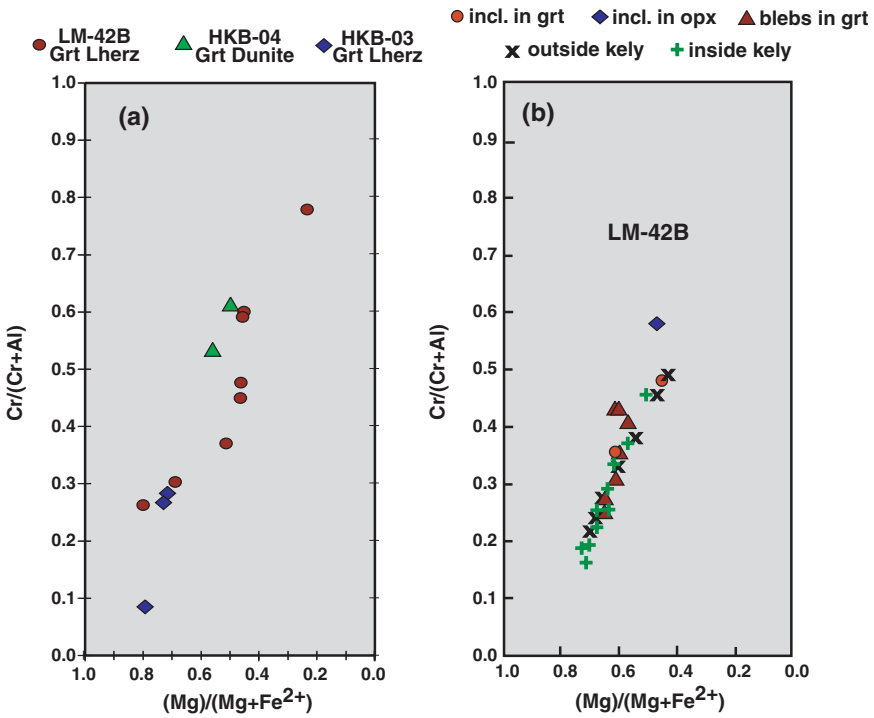

Fig. 10. Mg# versus Cr# in spinels from (a) peridotites LM-42B, HKB-3 and HKB-4 and (b) within peridotite LM-42B. See text for discussion.

$^{187}Re/^{188}Os$ ratios less than 5 (the less ^{187}Re, the more likely the measured $^{187}Os/^{188}Os$ ratio is reliable). The data are widely scattered (i.e. 1·3 Ga ± 0.4, MSWD = 325) both for individual samples and when all data are considered. A significant number of analyses (≈35 of 53) fall on or near a best-fit line that defines an age of ≈1·6 Ga, which is essentially the same time a mantle enrichment event re-fertilized WGC peridotites (Beyer *et al.*, 2006). A few sulfide analyses (≈10) plot along a shallower trend, probably related to crustal fluid introduction during Scandian recrystallization. The remaining (≈8) analyses have high $^{187}Os/^{188}Os$ ratios and lines fitted through each point yield meaningless ages older than the Earth. Several of these analyses, particularly from garnet lherzolite Camp 2–1, are robust with strong Os signals and resultant small errors (shown by small error ellipses) and very low ^{187}Re corrections. They define reasonable ages if it is assumed that the samples underwent a Re enrichment event (see below).

Model ages (Supplementary Data Table S4) are widely scattered, from ages older than the Earth to future ages. All future ages are eliminated when analyses with $^{187}Re/^{188}Os$ >0·5 and Os concentrations <10 ppb are excluded, but ages older than 4·55 Ga remain. These ages are modified if it is assumed that Re was introduced into Re-free Archean sulfides during an enrichment event (Table 6). Figure 15b plots ages that result if enrichment occurred at ≈1·6 Ga. The ages range between 2·1–4·1 Ga, with possible clusters between 2·4–2·8 and 3·5–4·1 Ga. Assigning enrichment at 1·6 Ga is based on evidence that peridotites in the WGC were enriched at that time (Beyer *et al.*, 2004, 2006, 2012) and the 1·6 Ga scatterchron defined by some sulfides (Fig. 15a). But the evidence for a 1·6 Ga event in the Tvaerdal peridotites is not strong and a younger enrichment would have resulted in the same reduction in the scatter of the model ages. A few pyroxenite sulfides do generate reasonable model ages without assuming Re-addition, but only those from EH-21 define straightforward model ages (CHUR) around 1.6 Ga. The data from Camp 2–1 sulfides are particularly interesting (Table 7) in that the Re/Os ratios are very low and the Os signals very strong. One analysis of sulfide in Camp 2–1-A has a particularly low $^{187}Os/^{188}Os$ ratio (0·09973, fractionation corrected) and generates very old Archean ages regardless of assumptions about Re-addition or depletion. The remaining analyses from this sample also generate Archean ages.

DISCUSSION

Origin of the Liverpool Land peridotites and pyroxenites

The Tvaerdal peridotite lenses have all the characteristics of mantle wedge peridotites (Brueckner & Medaris, 2000) and belong to the Mg–Cr type garnet peridotite class initially proposed by Carswell *et al.* (1983) for the WGC of Norway and orogenic peridotites worldwide (Bodinier & Godard, 2004). Most lenses are highly depleted garnet harzburgite and garnet dunite, the residues of extensive melt extraction. We suggest that melting removed most of the clinopyroxene, but not the

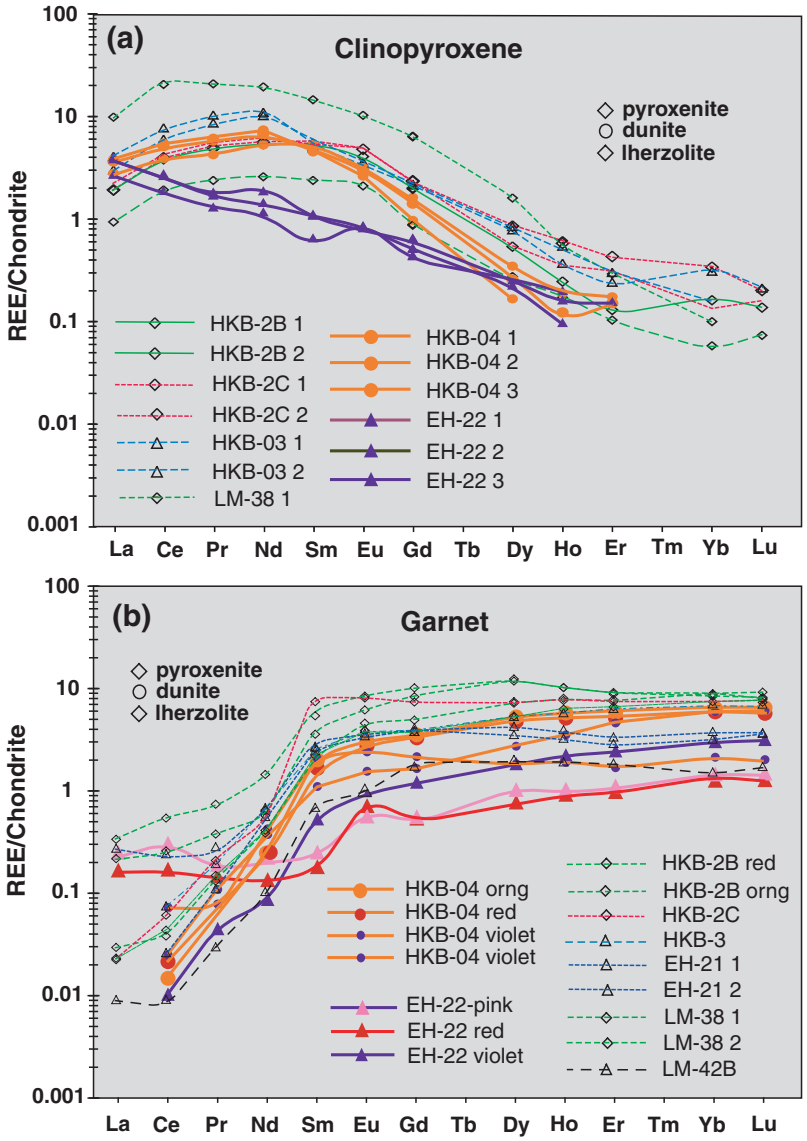

Fig. 11. REE patterns for (a) clinopyroxene and (b) garnet separated from Liverpool Land peridotites and pyroxenites, normalized to chondritic mantle (McDonough & Sun, 1995). Most clinopyroxenes show similar hooked patterns except for the straight pattern displayed by EH-22, a garnet wehrlite, which also shows a weak positive Eu anomaly for one grain. The garnet patterns are variable with some showing evidence of LREE enrichment and others none. Light coloured garnets from wehrlite EH-22 (filled triangles) show evidence of LREE enrichment but the dark one does not.

Cr-rich garnet that is scattered throughout the peridotite host (Fig. 2b and f) or occurs as thin trains separated by fine grained, recrystallized olivine (Fig. 2c and d). Re–Os results indicate that melt extraction episodes occurred throughout the Archean and Early Proterozoic (Fig. 15a and b) and it is possible that the garnets date back to these ancient events. Subsequent refertilization involving Re addition is required to avoid Re–Os model ages older than 4·55 Ga. One such event could have been through the introduction of pyroxenite melts, as has been proposed for the peridotites in the WGC (Beyer *et al.*, 2006). WGC garnet pyroxenites give Proterozoic recrystallization ages (Brueckner *et al.*, 2010 and references therein), but evidence for Proterozoic refertilization of the Tvaerdal peridotites is restricted to the ≈1·6 Ga errorchron generated by some sulphides on a Re–Os isochron diagram (Fig. 15a). More recent Re introduction could also generate reasonable Re–Os model ages and the LREE enrichment patterns of whole-rock and garnet and 'crustal' Sr–Nd isotope ratios of some clinopyroxenes (Figs 11 and 14) are consistent with a Scandian refertilization event that could have occurred in the mantle wedge from subduction zone fluids or from crustal fluids after the peridotite lenses were inserted into Tvaerdal Complex.

Pyroxenite evolution

The evolution of most Tvaerdal pyroxenites is relatively straightforward, albeit with some caveats. Some

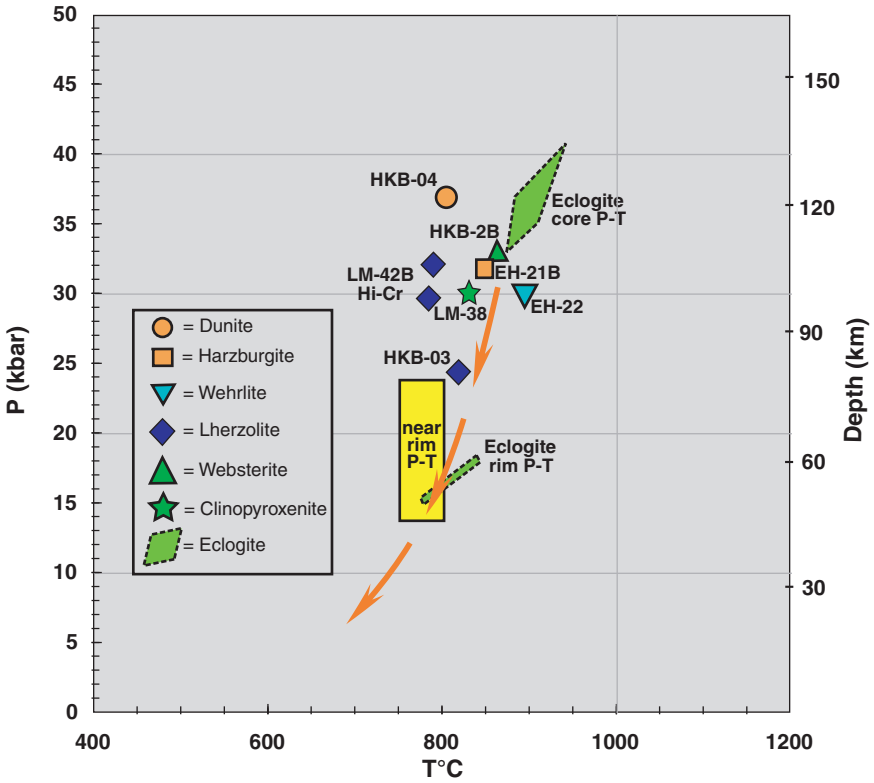

Fig. 12. *P–T* estimates for selected Tvaerdal peridotites and pyroxenites based on major element measurements from mineral cores and rims. Pyroxenite HKB-2B and harzburgite EH-21B plot close to the P–T estimate for an orthopyroxene-bearing eclogite in the host gneisses (Brueckner *et al.*, 2016). The pressures of pyroxenite LM-38 and wherlite EH-22 were set at 30 kbar in order to obtain temperatures. Peridotites, some of which are believed to contain two garnet generations, plot as more scattered points. See Supplementary Data Table S3C for complete data.

garnets in websterites HKB-2B and LM-43 give the same Scandian Sm–Nd ages (Fig. 13) as the eclogites in the enclosing gneisses (Brueckner *et al.*, 2016), indicating that the garnet pyroxenites recrystallized at the same time as the eclogites. This age correspondence suggests that the pyroxenites were inserted into the Tvaerdal crust as passengers within their peridotite hosts and continued recrystallizing at progressively higher pressures and temperatures during the subduction of the Tvaerdal Complex into the mantle (the 'prograde type' of Brueckner & Medaris, 2000). However, the only pyroxenite (websterite HKB-2B) analysed for *P-T* (Fig. 12) plots at a slightly lower pressure and temperature than that defined by the eclogites (Fig. 12), suggesting that it may have re-equilibrated as it was exhumed from mantle depths. Several peridotite samples plot close to the exhumation path defined by the Tvaerdal eclogites, suggesting that they also equilibrated during exhumation.

Re-equilibration at peak *P–T* and/or during subsequent retrogression appears to have erased most evidence for the prograde evolution of the pyroxenites, consistent with the flat concentration patterns across garnet grains for most major elements (Figs 8 and 9). Cr and Ca however are exceptions. Their concentrations increase from garnet core to rim in websterite HKB-2B (Figs 2k and 8a) as well as in most garnets from LM-42B (Fig. 9a). This increase is consistent with the progressive destruction of Cr-rich spinel to form Cr-garnet as *P–T* conditions increased during subduction through the reaction (O'Neill, 1981)

1. orthopyroxene + clinopyroxene + Cr-spinel → olivine + Cr-rich garnet

Trivalent Cr diffuses at a significantly slower rate in garnet than bivalent elements (diffusion coefficients are 0·5–1·5 $\log_{10}$ units smaller, Carlson, 2012). Therefore the re-equilibration that erased the prograde patterns of bivalent Mg, Fe, and Mn in most garnets was not intense enough to homogenize the profile defined by Cr. Ca^{++} would normally be expected to re-equilibrate to the same flat profiles defined by the other bivalent cations, but instead it replicates the Cr pattern (Fig. 8a and b). Reaction (1) forms garnet that is progressively richer in Ca at the expense of clinopyroxene. The rimward increase in Ca in garnet is probably the result of this transfer. Also, Ca diffuses more slowly in garnet than the other bivalent cations (diffusion coefficients for Ca are ≈0·5 $\log_{10}$ units smaller than for Mg, Fe^{++}, and Mn; Carlson, 2012; Fig. 10). If this reasoning is correct, the Cr and Ca profiles are the only elements that reflect the prograde evolution of the Tvaerdal garnet pyroxenites.

Table 5: Isotope data from garnet peridotite and pyroxenite Tvaerdal Complex, Liverpool Land

		Sr ppm	$^{87}Sr/^{86}Sr$	2 sigma	Sm ppm	Nm ppm	$^{147}Sm/^{144}Nd$	$^{143}Nd/^{144}Nd$	2 sigma
Camp 2-1 cpx	LDEO	72·7	0·704206	0·000010		1·13		0·513308	0·000018
HKB-2C cpx	LDEO	734	0·709850	0·000010	2·42	8·27	0·177	0·512253	0·000009
HKB-3 cpx	LDEO	289	0·705026	0·000007	3·13	20·4	0·093	0·511414	0·000007
HKB-4 cpx	LDEO	130	0·705963	0·000010	2·11	6·98	0·183	0·513038	0·000011
LM-42B cpx	SB	nm	0·704272	0·000002	1·031	3·65	0·171	0·513094	0·000008
LM-42B amph	SB	nm	0·704444	0·000013	nm	nm	nm	0·513201	0·000016
AA 08-47 cpx	SB	nm	0·7072713	0·000008	2·12	11·13	0·115	0·512105	0·000008
HKB 2B									
cpx 1	LDEO	197	0·706722	0·000010	2·56	9·46·	0·164	0·512234	0·000011
cpx2	LDEO	184	0·706708	0·000008	2·38	7·89	0·182	0·512267	0·000007
wr1	LDEO	nm	nm	nm	1·28	3·54	0·218	0·512388	0·000009
orange grt1	LDEO	nm	nm	nm	1·13	0·607	1·13	0·514904	0·000008
orange grt 2	LDEO	nm	nm	nm	1·127	0·589	1·16	0·514956	0·000007
red grt 2	LDEO	nm	nm	nm	1·17	0·690	1·02	0·514536	0·000021
red grt1	LDEO	nm	nm	nm	1·20	0·685	1·06	0·514764	0·000009
LM-43									
amph	SB	nm	0·705033	0·000002	0·592	1·486	0·241	0·513478	0·000006
cpx	SB	nm	0·703971	0·000010	2·033	6·822	0·180	0·513257	0·000006
wr	SB	nm	nm	nm	0·756	2·066	0·221	0·513397	0·000006
grt 2	SB	nm	nm	nm	0·380	0·204	1·13	0·515804	0·000060
grt 3 light	SB	nm	nm	nm	0·425	0·226	1·14	0·51817	0·000009
grt 3 dark	SB	nm	nm	nm	0·356	0·192	1·12	0·515685	0·000010
EH-22									
cpx1	LDEO	181	0·703961	0·000008	0·430	1·99	0·130	0·512976	0·000017
cpx2	LDEO	170	0·703902	0·000008	0·427	1·95	0·132	0·513012	0·000010
dark grt	LDEO	nm	nm	nm	0·169	0·120	0·855	0·516804	0·000019
dark grt2	LDEO	nm	nm	nm	nm	0·102		0·516717	0·000017
pale grt	LDEO	nm	nm	nm	0·146	0·100	0·888	0·516192	0·000015
pale grt 2	LDEO	nm	nm	nm	0·211	0·149	0·856	0·516301	0·000027
wr	LDEO	nm	nm	nm	0·149	0·579	0·155	0·513031	0·000106
wr2	LDEO	nm	nm	nm	0·218	0·846	0·156	0·513064	0·000015
LEA 08-04									
cpx	LDEO	nm	nm	nm	1·762	7·193	0·148	0·512632	0·000008
cpx2	LDEO	171	0·70751	0·000010	1·649	6·754	0·148	0·512601	0·000007
wr	LDEO	nm	nm	nm	0·623	2·20	0·171	0·512693	0·000008
pink grt2	LDEO	nm	nm	nm	0·499	0·364	0·830	0·51434	0·000050
pink grt	LDEO	nm	nm	nm	0·545	0·292	1·130	0·51535	0·000022
orange grt	LDEO	nm	nm	nm	0·448	0·269	1·010	0·516759	0·000017
orange grt2	SB	nm	nm	nm	0·559	0·333	1·018	0·516726	0·000017

Analyses at Lamont Doherty Earth Observatory (LDEO) and Stony Brook (SB). nm, not measured.

Peridotite evolution

In contrast to the apparent solely Scandian history of the LL garnet pyroxenites, the mixed garnet assemblages within some garnet peridotites appear to require two widely separated metamorphic events and a mechanism for mixing these assemblages. There are two garnet generations in all three peridotite samples which we studied in detail, LM-42B, EH-22 and LEA 08–04. They all contain mixtures of Cr-rich and Cr-poor garnet and the two dated samples define two age clusters with Cr-rich dark garnets much older than Cr-poor garnets (LM-42B lacked sufficient clinopyroxene to obtain a Sm–Nd mineral age). A Cr-poor garnet aliquot of one peridotite (LEA 08–04) gave an age (384 ± 32 Ma; Fig. 13d) that is within error of the Scandian ages obtained from garnet pyroxenites (Fig. 13a and b) and eclogites (Brueckner *et al.*, 2016). Therefore we provisionally label these assemblages M_2. The high-Cr garnets are suggested to be the refractory garnets that occur within dunite and harzburgite (discussed above) as suggested by their older (minimum) ages in the mixed assemblages (Fig. 13c and d). These refractory garnets could not be dated directly by Sm–Nd because of the general paucity of clinopyroxene in dunite and harzburgite. However, the Re–Os evidence presented above suggests they originated during the Archean or Proterozoic. Refractory garnets in dunites and harzburgites give mixed, but generally high Cr contents (1·1 to 5·0 wt % Cr_2O_3, Table 4). Thus we propose the high-Cr garnets in the mixed assemblages are also refractory garnets and we label them M_1. We further propose that the M_1 garnets in all dunites, harzburgites and lherzolites were originally larger porphyroclasts that had steep core to rim gradients in Cr content. Fracturing these porphyroclasts into smaller dispersed fragments would explain the large variation in Cr content between individual grains (note for example variations between different coloured garnets in Table 4). It might also explain the variations in Mg-number between garnet grains in sample LM-42B (Fig. 9b). This model is discussed further below.

We suggest that fragmentation and dispersal can also provide a mechanism for the mixing of Cr-poor and Cr-rich garnets observed in some samples. We

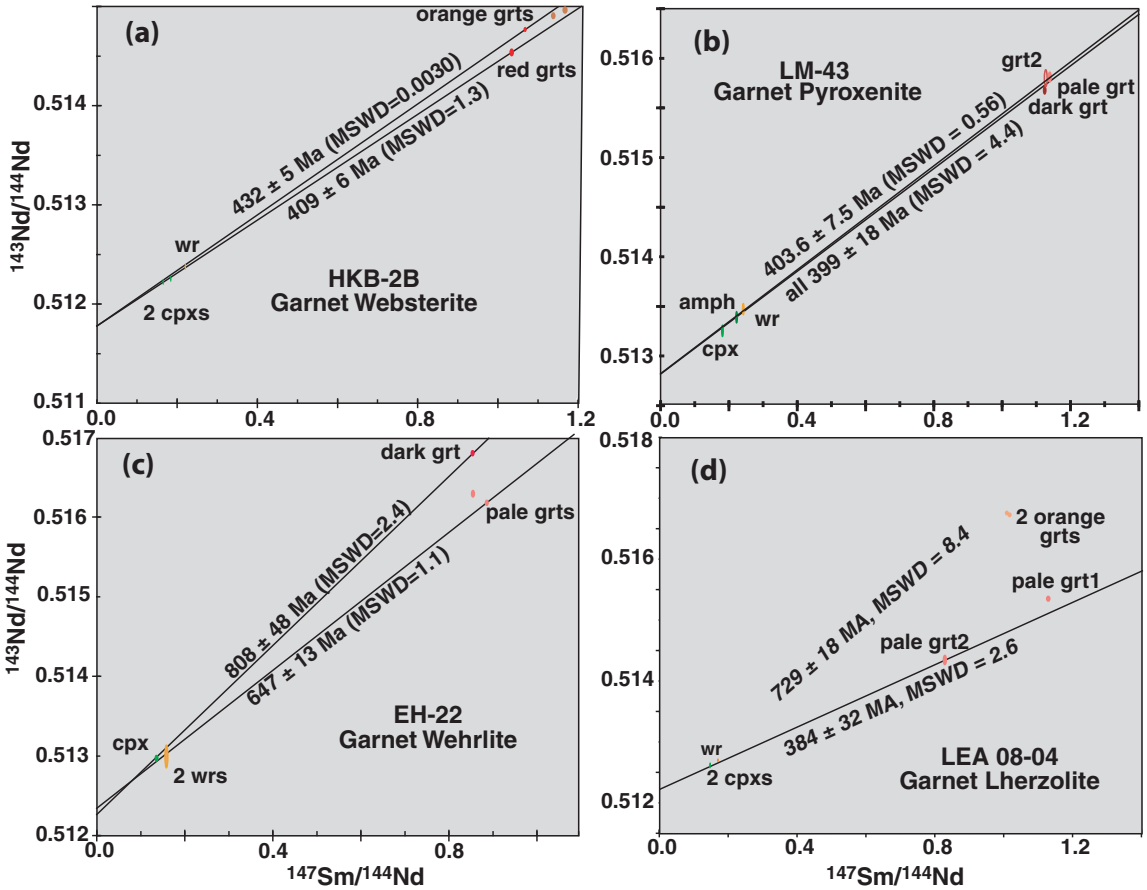

Fig. 13. Garnet–clinopyroxene–whole-rock Sm–Nd isochron diagrams. (a) Pyroxenite HKB-2B and (b) LM-43 give a relatively narrow age span for garnets of different colours, suggesting that a single garnet generation grew or re-equilibrated over ≈20 million years during the Scandian orogeny. The much larger age difference between different coloured garnets in (c) wehrlite EH-22 and (d) LEA 08–04 indicates two separate garnet-forming events. The youngest age for a pale garnet from LEA 08–04 (d) represents a valid Scandian date, but with a large error.

propose the Cr-poor garnets were mixed in from dismembered pyroxenites that also fragmented as a result of extreme shearing during the Scandian orogeny. Support for the mixing model is as follows: (1) the two garnet generations have different Cr concentrations (Fig. 9a); (2) they show a bimodal distribution in apparent ages (Fig. 13c and d), indicating two garnet-forming events; the lighter garnets should give younger ages than the darker garnets if they were derived from young (Scandian) pyroxenites; (3) many garnet grains are blocky, angular and irregular and show a range of sizes, suggesting they are fragments of earlier larger gains (see further discussion below); (4) large garnets with symmetric Cr profiles would break into smaller grains with different Cr contents and the observed asymmetric profiles (Figs 8 and 9); (5) rotation and flattening during shearing and/or shortening could explain the striking parallelism of garnet pyroxenite and peridotite layers and M_1 garnet trains (Fig. 2c–f) in all peridotite lenses; (6) the C-type fabric determined from LM-42B (Luc Mehl, personal communication) is consistent with such large strains; (7) some garnet-rich trains are remarkably thin, one or two minerals wide (Fig. 2c, d and h), which could also be the result of extreme shearing; (8) thicker garnet pyroxenite layers that have remained coherent (i.e. Fig. 2l) nevertheless show locally fractured garnets with pieces that have moved apart (Fig. 2i, j and k).

A possible problem with this mixing model is that M_2 clinopyroxene and orthopyroxene from dismembered pyroxenites should also have been mixed in along with garnets. We measured the compositions of five clinopyroxenes from sample LM-42B (Fig. 7b) and none of them have the Cr-poor compositions expected of clinopyroxenes from pyroxenites. However, neither do they have the Cr-rich compositions of clinopyroxenes from dunite, harzburgite and another lherzolite (Fig. 7b). Instead they occupy an intermediate composition, which suggests that they might have re-equilibrated during Scandian recrystallization.

Mixed assemblages with M_2 clinopyroxene and Cr-poor garnet and M_1 Cr-rich garnet and olivine (no or few M_1 clinopyroxenes) would lead to spurious mineral isochron ages. If the clinopyroxene is solely from pyroxenite (i.e. M_2) the mixing of it with garnets of two different ages (M_1 and M_2) would most likely result in a minimum age for the older event. However, depending

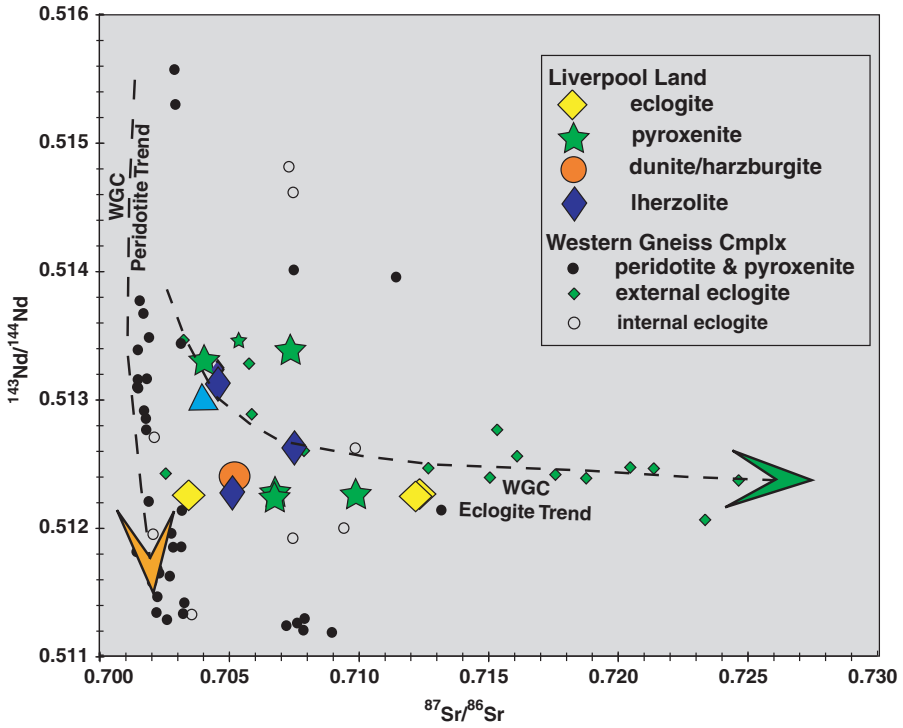

Fig. 14. $^{143}Nd/^{144}Nd$-$^{87}Sr/^{86}Sr$ covariance diagram for clinopyroxenes and two amphiboles (smaller symbols) from Liverpool Land eclogites (diamonds), pyroxenites (stars), dunites (circles) and lherzolites (triangles). Values for eclogites (Brueckner, unpublished) and garnet peridotites and pyroxenites from the WGC (Brueckner *et al.*, 2010) are plotted for comparison. The LL clinopyroxenes show evidence of crustal contamination (high $^{87}Sr/^{86}Sr$, low $^{143}Nd/^{144}Nd$) relative to most peridotites in the WGC. The few clinopyroxenes from WGC peridotites with high $^{87}Sr/^{86}Sr$ and low $^{143}Nd/^{144}Nd$ are from M_3 (Scandian) assemblages.

Table 6: Re–Os data for peridotite and pyroxenites, Tvaerdal Complex, Liverpool Land

Sample	description	$^{187}Os/^{188}Os$	±	$^{187}Re/^{188}Os$	±	CHUR	RD at 1·6 Ga	RE at 1·6 Ga	Os ppb	185Re ppb
CHUR		0·1270		0·423		0	0·00	1·69		
LL06 EH-21	s1A	0·1179	0·0006	0·014	0·003	1·40	1·35	1·40	28·0	0·08
"	s1B	0·1218	0·0004	0·149	0·012	1·21	0·77	1·35	11·6	0·13
"	s1C	0·1216	0·0008	0·212	0·002	1·68	0·80	1·64	7·38	0·12
"	S4A	0·1162	0·0021	0·245	0·008	4·00	1·59	2·57	5·37	0·10
LL06 EH-22	3A	0·1143	0·0003	0·148	0·007	2·93	1·87	2·47	3·90	0·04
"	1B	0·1092	0·0024	0·275	0·013	7·88	2·60	3·71	2·40	0·04
"	1C	0·1192	0·0033	0·225	0·013	2·59	1·15	2·05	1·95	0·03
Camp 2-1-A	fractionated	0·1086	0·0004	0·294	0·009	9·44	2·69	3·87	19·9	0·21
Camp 2-1-A	corrected	0·0997	0·0012	0·036	0·012	4·31	3·94	4·14	74·6	0·15
Camp 2-1-A	"	0·1083	0·0003	0·298	0·008	9·94	2·74	3·93	19·5	0·22
Camp 2-1-H	"	0·1083	0·0002	0·172	0·003	4·69	2·73	3·43	18·6	0·12
Camp 2-1-H	"	0·1080	0·0003	0·161	0·003	4·57	2·78	3·44	21·9	0·13
Camp 2-1-H	"	0·1081	0·0005	0·185	0·003	5·02	2·76	3·52	14·8	0·10
Camp 2-1-I	"	0·1079	0·0001	0·028	0·001	2·99	2·79	2·93	137	0·15
Camp 2-1-I	"	0·1082	0·0001	0·038	0·002	3·02	2·74	2·92	99·8	0·13
Camp 2-1-I	"	0·1082	0·0003	0·020	0·004	2·89	2·74	2·85	511	0·10
Camp 2-1-I	"	0·1096	0·0003	0·067	0·002	3·04	2·54	2·83	30·1	0·08
Camp 2-1-I	"	0·1083	0·0004	0·030	0·003	2·95	2·73	2·88	132	0·08
Camp 2-1-5	"	0·1182	0·0005	0·245	0·016	3·27	1·30	2·28	15·8	?
Camp 2-1-15	"	0·1076	0·0005	0·314	0·012	12·03	2·83	4·09	21·0	?
Camp2-bl1-1	"	0·1084	0·0020	0·851	0·036	−2·54	2·72	6·03	5·80	?
Camp2-bl1-8	"	0·1076	0·0009	0·223	0·009	6·18	2·83	3·74	11·6	?

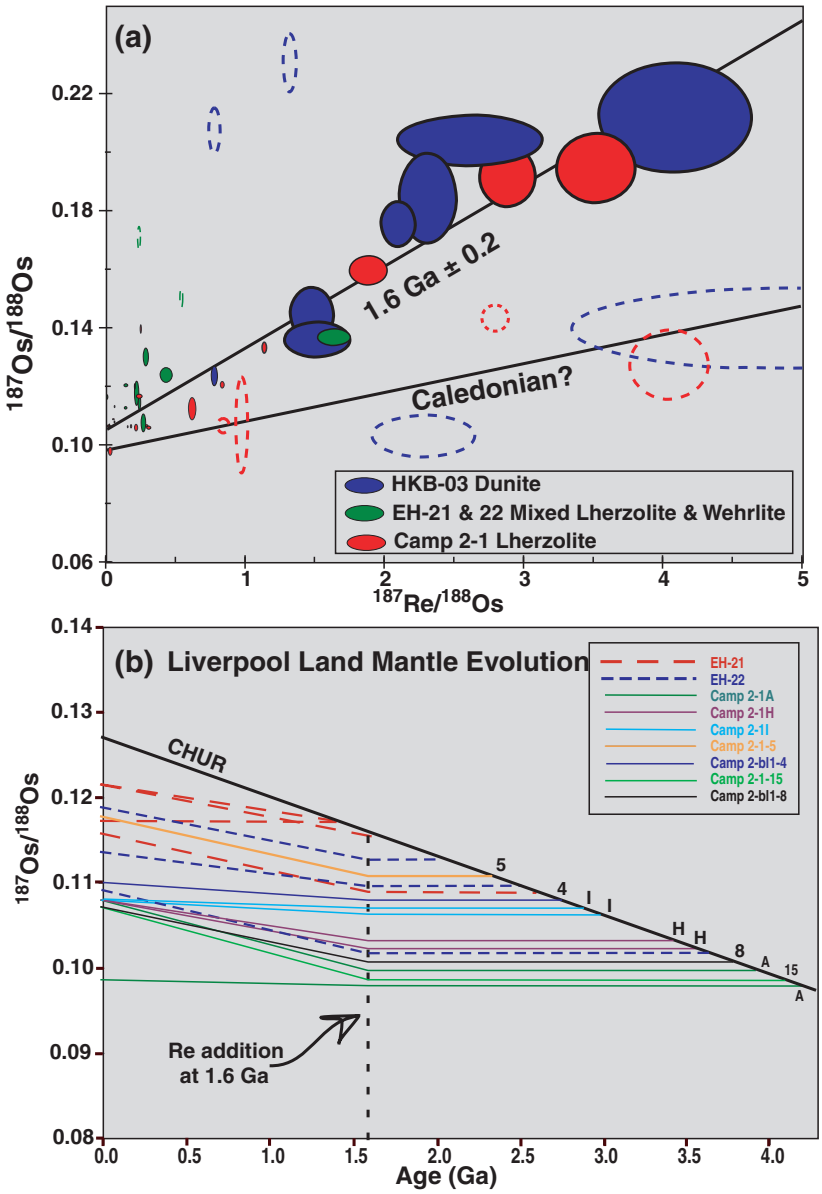

Fig. 15. (a) Re–Os isochron diagram for LA-ICP-MS analysed sulfides from Liverpool Land peridotites and pyroxenites. Symbols with dashed borders were excluded from calculating the ≈ 1·6 Ga errorchron. (b) $^{187}Os/^{188}Os$ evolution diagram for sulfides with low $^{187}Re/^{188}Os$ ratios and present day $^{187}Os/^{188}Os$ ratios below CHUR, assuming Re enrichment at 1·6 Ga. The letters and numbers at the intercepts of Camp 2–1 sulfides with the CHUR line refer to separate sulfides within the dunite, which otherwise would give ages older than the Earth. Repeated letters refer to maximum and minimum ages from individual sulfides (see Supplementary Data Table S4).

on the relative proportions of M_1 and M_2 garnet, the apparent ages could be older, younger and even, by serendipity, the same age as the earlier garnet-forming event. Therefore the two sets of Sm–Nd ages defined by minerals from EH-22 and LEA 08–04 (Fig. 13c and d) yield no precise information on their time of formation, except for the Scandian age of the pale garnet in LEA 08–04, which appears to be an aliquot of M_2 garnets almost completely separated from M_1 garnets. Similar arguments suggest that the *P–T* estimates from LM-42B could be invalid. For example, the Al-in-orthopyroxene geobarometer could potentially pair a M_2 orthopyroxene with a M_1 garnet or *vice versa* (this problem was largely avoided by analysing cores and rims of adjacent grains in several domains in the rock sample).

The mechanical mixing of two garnet-bearing assemblages of different age resolves many of the problems that arise if the garnets had formed during a single metamorphic cycle. However, certain conditions would have had to be in place for which there is little direct evidence. For example, postulating the existence of large parental M_1 grains would explain the large inter-grain variation in the Cr content (and Mg-number) of garnets in sample LM-42B (Fig. 9). It would also

explain why the Cr-rich (darker) garnets in EH-22 and LEA 08–04 give older ages than the Cr-poor (i.e. lighter) garnets. Cr content increases from core to rim in most other measured samples (Fig. 8) and so paler cores should give older ages than darker rims, but the opposite is true. The solution is two metamorphic events, with both events producing core to rim gradients in Cr concentrations. The first event (M_1) generated negative core to rim Cr gradients in garnet as a result of decreasing *P–T* conditions, perhaps as a result of decompression within a mantle plume. The core to rim decrease in pyrope and increase in almandine content of the Cr-rich garnet in LM-42B (GM 1 in Fig. 9b) is consistent with this hypothesis. The result would be a large difference in Cr concentration between the core and rim, but within large garnets, resulting in Cr gradients with relatively shallow slopes (the larger the grain, the shallower the slope). The scan of the Cr-rich garnet in LM-42B (GM 1 in Fig. 9a) might be from the core of such a garnet as it is the only measured garnet that displays a convincing symmetrical core to rim decrease in Cr content. Fragmenting these garnets would produce smaller grains, each displaying a fraction of the original profile (Fig. 9b). Thus different grains would have different Cr concentrations (and colours) depending on where they originally occurred in the parent grain (i.e. dark fragments from the core, light fragments from the rim). These fragments would also inherit the shallow Cr-profiles of the parental grain and, therefore, not show much internal colour change, while still showing visible colour differences between grains.

The second required recrystallization event (M_2), presumably Scandian metamorphism, imposed new zoning patterns for Cr at the same time the parent garnets broke into smaller fragments as a result of shearing. Each fragment would have preserved the overall Cr content of its position in the original porphyroclast, but with a new imposed M_2 gradient. Most grains show a core to rim increase in Cr concentration, so the new gradient probably formed during prograde metamorphism (i.e. Equation 1). Further fragmentation would break these grains into still smaller grains, many with incomplete (asymmetric) profiles. Stated succinctly, grain-to-grain variations in Cr content reflect gradients generated in the precursor porphyroclast during M_1 metamorphism, but intra-grain variations reflect gradients in fragments of these porphyroclasts during M_2 (Scandian) metamorphism. The large parental porphyroclasts hypothesized in this model (>10 cm) have not been observed in the peridotites of the Tvaerdal Complex. The largest M_1 garnet measured is 2 cm wide. However, such porphyroclasts >10 cm wide have been described in the peridotites of the northwestern WGC (Spengler, *et al.*, 2009; Van Roermund, 2009a,b).

The trivalent REE elements presumably developed core to rim patterns similar to those of Cr^{+++}. These gradients could explain the variations in the obtained Sm–Nd mineral ages (Fig. 13). REE in the cores of the parental porphyroclasts would be least affected by subsequent re-equilibration and, therefore, tend to preserve older ages. The more completely equilibrated areas near the rim would give younger ages. But the garnets from the parental cores would be at least partially re-equilibrated, resulting in minimum M_1 ages, and the garnets from the rims would not equilibrate completely, resulting in maximum M_2 ages. Dating garnet fragments produced by this mechanism would give older ages for the cores (dark garnets) and younger ages for the rims (pale garnets), which is what is observed.

The mixing of M_1 and M_2 assemblages appears to have generated some peridotites with whole-rock compositions within or near the lherzolite field (Table 3, Fig. 3). Lherzolites are classically interpreted as samples of primitive mantle (Bodinier & Godard, 2004). More recently some lherzolites have been shown to be the result of metasomatism (Su *et al.*, 2016), even in the classic type locality (i.e. Lherz; La Roux *et al.*, 2007). The mechanical mixing model offers yet another hypothesis to explain the compositions of LL lherzolites, olivine websterites, and wehrlites.

A COMPARISON OF TVAERDAL PERIDOTITES WITH WGC PERIDOTITES

If the Tvaerdal Complex is a stranded Baltic terrain, identical in age, tectonic position and history to the WGC of Norway, it follows that the peridotites within them might have had a common origin and history. There are similarities, but also significant differences. Re–Os data suggest both ultramafic assemblages originated from a mixed Archean/Proterozoic mantle (Beyer *et al.*, 2004), consistent with a Laurentian mantle wedge above subducted Baltica (Brueckner *et al.*, 2010, Fig. 7; Beyer *et al.*, 2012). The WGC garnet assemblages that are most similar to those in LL may be the spectacular 'relict-type' garnet peridotites and garnet pyroxenites (Brueckner & Medaris, 2000) of the northwestern WGC (Spengler *et al.*, 2006; 2009; Van Roermund, 2009a,b; Brueckner *et al.*, 2010; Scambelluri *et al.*, 2010). These peridotites and their host gneisses were subducted to the deepest level of the mantle during the terminal collision of Baltica and Laurentia where they generated Scandian-age garnets (correlated here with the M_2 garnets in the Tvaerdal pyroxenites). Additionally, the WGC ultramafics also contain older garnet assemblages; M_1 and M_2 garnets generated in the mantle during the Archean and Proterozoic, respectively. The WGC M_1 garnets formed initially as very large porphyroblasts, as has been proposed above for the M_1 Cr-rich Tvaerdal garnets. However the maximum errorchron age generated by M_1 garnets in LL peridotites is only 808 Ma (Fig. 13), much younger than the oldest ages (≈1·6 Ga) defined by M_2 garnets in WGC peridotites and pyroxenites (Brueckner *et al.*, 2010). Sm–Nd clinopyroxene isotope variations and Re–Os sulfide model ages from the Tvaerdal peridotites (Figs 14 and 15; Tables 5 and 6) suggest they experienced a mantle fertilization

event, similar to that which affected the peridotites of the WGC (Beyer *et al.*, 2004, 2006). However the Tvaerdal peridotites lack convincing evidence that this event occurred in the mantle at ≈1–6 Ga as was the case in the WGC. A final conclusion on the relationships between these ultramafic occurrences requires considerably more research, but the overall impression so far is each association has its own unique petrogenetic history, suggesting either the (Laurentian?) mantle wedge from where they were derived was strikingly heterogeneous or there was more than one mantle wedge beneath potentially different overriding terranes.

CONCLUSIONS

Six garnet peridotite lenses occur within the gneisses of the HP/UHP Tvaerdal Complex in Liverpool Land, Greenland Caledonides. The peridotites are predominantly dunite and harzburgite, but include layers of strikingly parallel lherzolite, websterite and wehrlite. Several samples include two garnet populations, one older and Cr-rich (M_1) and the other younger (≈400 Ma) and Cr-poor (M_2). We propose the two garnet populations in these samples were mechanically mixed through intense shearing during the Scandian orogeny. Evidence for this intense shearing includes: garnet grains that are fractured, separated and locally disaggregated; garnets that have asymmetric edge-to-edge gradients in Cr and Ca content; garnet grains that are strung out in thin layers; striking variations in Cr content in neighboring garnet grains; and the parallelism of all pyroxenite, peridotite and garnet-rich layers. The M_2 garnets were probably derived from disaggregated pyroxenite layers. The source of the M_1 garnets is less certain, but we suggest they are disaggregated fragments of refractory garnet porphyroclasts that were left behind after Archean and/or Proterozoic melting events in the mantle. The intense shearing that fragmented garnet porphyroclasts and thin pyroxenite veins, and locally mixed their assemblages, simultaneously thinned the layers and rotated them into parallelism. Clinopyroxenes within these mixed rocks, unlike the garnets, do not plot as two populations. Either most M_1 clinopyroxene was removed during Precambrian melting or mixed M_1 and M_2 clinopyroxenes re-equilibrated with each other to form clinopyroxenes with intermediate compositions.

Garnets and other minerals within thick (>5 cm) pyroxenite layers appear to have remained coherent and contain only M_2 assemblages. *P–T–t* results from these pyroxenites, combined with earlier studies of LL eclogites within the adjacent gneisses, are consistent with the subduction of the Tvaerdal Complex around 400 Ma ago to mantle depths of ≈110–120 km and temperatures of 850–900°C. The similar Scandian history of eclogite and garnet pyroxenite, which had very different origins, indicates that the peridotite lenses were inserted from the mantle wedge into the Tvaerdal Complex relatively early, during subduction, resulting in the subsequent shared history. Recrystallization under peak HP/UHP conditions resulted in the nearly complete equilibration of M_2 garnet-bearing assemblages in the pyroxenites: only Cr and Ca profiles may record a prograde history. The exhumation of the Tvaerdal Complex brought it against the lower crustal Jaettedal Complex, resulting in a transfer from Baltica to Laurentia. Subsequently both complexes moved towards the surface along the Grubbedalen Shear Zone.

Mechanical peridotite/pyroxenite mixing may be a more important process than generally realized. A critical question is where such mixing occurred: within the mantle or later, after introduction into the subducted crust? If in the mantle, the mechanical mixing model has consequences for understanding the geochemical evolution of the mantle where most variations in mantle composition are assumed to be the result of melting and, or, chemical processes.

ACKNOWLEDGEMENTS

Hannes Brueckner and Scott Johnston are grateful to Ebbe Hartz, who invited us to join field excursions in LL in the summers of 2006 and 2007 with equipment provided by him and expenses covered by Statoil ASA. We thank Luc Mehl, Kenjo Agustsson and Richard Bubbico for assistance with fieldwork and Aka Lynge for assistance with field logistics. Luc Mehl also measured LPO olivine and orthopyroxene fabrics and Richard Bubbico assisted in sample preparation and analysis. We are also very grateful to many people who supported this research and helped us acquire and manipulate the data presented herein; specifically Suzanne O'Reilly and Norman Pearson (MU), Juliane Gross and Kennet Flores (AMNH), and Terry Plank and Louise Bolge (LDEO). Finally we thank Shuguang Song, Iwona Klonowska and an unnamed reviewer for helpful comments and suggestions.

This is contribution 8242 of the Lamont-Doherty Earth Observatory of Columbia University, contribution 1196 of the ARC Centre of Excellence for Core to Crust Fluid Systems (http://www.ccfs.mq.edu.au) and contribution 1247 of the GEMOC Key Centre (http://www.gemoc.mq.edu.au) and is related to IGCP-662.

FUNDING

This research was supported by The City University of New York Faculty Research Award Grants 66287–00 35, 67663–00 36, and 68556–00 37 to HKB and by National Science Foundation EAR 08–38530 to HKB and SJ.

SUPPLEMENTARY DATA

Supplementary data are available at *Journal of Petrology* online.

REFERENCES

Al-Samman, A. H. (1985). Mineralogy and geochemistry of ultramafic rocks in the west Norway basement gneiss terrain. Ph.D. thesis, University of Sheffield, Sheffield.

Andersen, T. B., Jamtveit, B., Dewey, J. F. & Swensson, E. (1991). Subduction and eduction of continental crust: major mechanisms during continent-continent collision and orogenic extensional collapse, a model based on the southern Norwegian Caledonides. *Terra Nova* **3**, 303–310.

Augland, L. E., Andresen, A. & Corfu, F. (2010). Age, structural setting, and exhumation of the Liverpool Land eclogite terrane, East Greenland Caledonides. *Lithosphere* **2**, 267–286.

Augland, L. E., Andresen, A. & Corfu, F. (2011). Terrane transfer during the Caledonian orogeny: Baltican affinities of the Liverpool Land Eclogite Terrane in East Greenland. *Journal of the Geological Society* **168**, 15–26.

Augland, L. E., Andresen, A., Corfu, F. & Daviknes, H. K. (2012). Late Ordovician to Early Silurian ensialic magmatism in Liverpool Land, East Greenland: new evidence extending the northeastern branch of the continental Laurentian magmatic arc. *Geological Magazine* **149**, 561–577.

Beyer, E. E., Brueckner, H. K., Griffin, W. L. & O'Reilly, S. Y. (2012). Laurentian provenance of Archean mantle fragments in Proterozoic Baltic crust of the Norwegian Caledonides. *Journal of Petrology* **53**, 1357–1383.

Beyer, E. E., Brueckner, H. K., Griffin, W. L., O'Reilly, S. Y. & Graham, S. (2004). Archean mantle fragments in Proterozoic crust, Western Gneiss Region, Norway. *Geology* **32**, 609–612.

Beyer, E. E., Griffin, W. L. & O'Reilly, S. Y. (2006). Transformation of Archaean lithospheric mantle by refertilization: evidence from exposed peridotites in the Western Gneiss Region, Norway. *Journal of Petrology* **47**, 1611–1636.

Bodinier, J.-L. & Godard, M. (2004). Orogenic, ophiolitic, and abyssal peridotites. In: Holland, H. D. and Turekian, K. K. (eds) *Treatise on Geochemistry*. Amsterdam: Elsevier, pp. 103–170.

Brueckner, H. K., Carswell, D. A., Griffin, W. L., Medaris, L. G., Jr, Van Roermund, H. L. M. & Cuthbert, S. J. (2010). The mantle and crustal evolution of two garnet peridotite suites from the Western Gneiss Region, Norwegian Caledonides: an isotopic investigation. *Lithos* **117**, 1–19.

Brueckner, H. K. & Medaris, L. G., Jr (2000). A General Model for the Intrusion and Evolution of "Mantle" Peridotites in High-Pressure and Ultrahigh-Pressure Metamorphic Terranes. *Journal of Metamorphic Geology* **18**, 119–130.

Brueckner, H. K., Medaris, L. G., Jr, Belousova, E. A., Johnston, S. M., Griffin, W. L., Hartz, E. H., Hemming, S., Ghent, E. & Bubbico, R. (2016). An orphaned baltic terrane in the Greenland Caledonides: a Sm-Nd and detrital zircon study of a high-pressure/ultrahigh-pressure complex in Liverpool Land. *The Journal of Geology* **124**, 541–567.

Brueckner, H. K. & Van Roermund, H. L. M. (2004). Dunk Tectonics: a multiple subduction/eduction model for the evolution of the Scandianvian Caledonides. *Tectonics* **23**, 1–20.

Carlson, W. D. (2012). Rates and mechanism of Y, REE, and Cr diffusion in garnet. *American Mineralogist* **97**, 1598–1618.

Carswell, D. A. (1966). Some ultrabasic bodies and related rocks in Sunnmöre, South Norway. Ph.D. thesis, University of Sheffield, Sheffield.

Carswell, D. A. (1968a). Picritic magma-residual dunite relationships in garnet peridotite at Kalskaret near Tafjord, southern Norway. *Contributions to Mineralogy and Petrology* **19**, 97–124.

Carswell, D. A. (1968b). Possible primary upper mantle peridotite in Norwegian basal gneiss. *Lithos* **1**, 322–355.

Carswell, D. A. (1973). Garnet pyroxenite lens within Ugelvik layered garnet peridotite. *Earth and Planetary Science Letters* **20**, 347–352.

Carswell, D. A., Harvey, M. A. & Al-Samman, A. (1983). The petrogenesis of contrasting Fe–Ti and Mg–Cr garnet peridotite types in the high-grade gneiss complex of western Norway. *Bulletinin de Minéralogie* **106**, 727–750.

Carswell, D. A., Van Roermund, H. L. M. & Wiggers de Vries, D. F. (2006). Scandian ultrahigh-pressure metamorphism of Proterozoic basement rocks on Fjørtof and Otrøy, Western Gneiss Region, Norway. *International Geology Review* **48**, 957–977.

Cheeney, R. F. (1985). The plutonic igneous and high-grade metamorphic rocks of southern Liverpool Land, central East Greenland, part of a supposed Caledonian and Precambrian complex. *Grønlands Geologiske Undersøgelse, Rapport* **123**, 1–39.

Coe, K. (1975). The Hurry Inlet granite and related rocks of Liverpool Land, East Greenland. *Bulletin Grønlands Geologiske Undersøgelse* **115**, 1–34.

Corfu, F. & Hartz, E. H. (2011). U–Pb geochronology in Liverpool Land and Canning Land, East Greenland—the complex record of a polyphase Caledonian orogeny. *Canadian Journal of Earth Sciences* **48**, 473–494.

Eskola, P. (1921). On the eclogites of Norway. *Videnskapsselskapets Skrifter. I. Mathematisk–naturvidenskabelig Klasse* **8**, 1–121.

Gasser, D. (2014). The Caledonides of Greenland, Svalbard and other arctic areas: status of research and open questions. In: Corfu, F., Gasser, D. & Chew, D. M. (eds) *New Perspectives on the Caledonides of Scandinavia and Related Areas*, **Volume 390**. London: Geological Society Special Publications, pp. 93–129.

Gee, D. G., Fossen, H., Henriksen, N. & Higgins, A. K. (2008). From the early Paleozoic platforms of Baltica and Laurentia to the Caledonide Orogen of Scandinavia and Greenland. *Episodes* **31**, 44–51.

Gee, D. G., Janák, M., Majka, J., Robinson, P. & van Roermund, H. (2012). Subduction along and within the Baltoscandian margin during closing of the Iapetus Ocean and Baltica-Laurentia collision. *Lithosphere* **5**, 169–178.

Hacker, B. R., Andersen, T. B., Johnston, S., Kylander-Clark, A. R. C., Peterman, E. M., Walsh, E. O. & Young, D. (2010). High-temperature deformation during continental-margin subduction and exhumation: the ultrahigh-pressure Western Gneiss Region of Norway. *Tectonophysics* **480**, 149–171.

Harley, S. L. (1984). An experimental study of the partitioning of Fe and Mg between garnet and orthopyroxene. *Contributions to Mineralogy and Petrology* **86**, 359–373.

Hartz, E. H., Condon, D., Austrheim, H. & Erambert, M. (2005). Rediscovery of the Liverpool Land Eclogites (Central East Greenland): a post supra-subduction UHP province. *Abstract, Mitteilungen der Österreichischen Mineralogischen Gesellschaft* **150**.

Hartz, E. H., Podladchikov, Y. Y. & Dabrowski, D. (2007). Tectonic and reaction overpressures: theoretical models and natural examples. *Abstract, European Geophysical Union General Assembly*, EGU2007-A-10430.

Higgins, A. K., Gilotti, J. A. & Smith, M. P. (eds) (2008). The Greenland Caledonides: Evolution of the Northeast Margin of Laurentia, **Volume 202**. *Geological Society of America Memoir*, pp. 1–368. doi:10.1130/2008.1202.

Johnston, S. M., Hartz, E. H., Brueckner, H. K. & Gehrels, G. E. (2010). U–Pb zircon geochronology and tectonostratigraphy of southern Liverpool Land, East Greenland: implications for deformation in the overriding plates of continental collisions. *Earth and Planetary Science Letters* **297**, 512–524.

Johnston, S. M., Kylander-Clark, A. & Brueckner, H. K. (2015). Migmatite gneiss of the Jættedal Complex, Liverpool Land, East Greenland: protracted high-T metamorphism in the

overriding plate of the Caledonian orogen. *Journal of Metamorphic Geology* **1**, 22.

Krogh, E. J. (1977). Evidence for a Precambrian continent-continent collision in western Norway. *Nature* **267**, 17–19.

Lappin, M. A. (1974). Eclogites from the Sunndal-Grubse ultramafic mass, Almklovdalen, Norway and the T-P history of the Almklovdalen masses. *Journal of Petrology* **15**, 567–601.

La Roux, V., Bodinier, J.-L., Tommasi, A., Alard, O., Dautria, J.-M., Vauchez, A. & Riches, A. J. V. (2007). The Lherz spinel lherzolite: refertilized rather than pristine mantle. *Earth and Planetary Science Letters* **259**, 599–612.

McDonough, W. F. & Sun, S.-S. (1995). The composition of the Earth. *Chemical Geology* **120**, 223–253.

Majka, J., Rosén, A., Janák, M., Froitzheim, N., Klonowska, I., Manecki, M., Sasinková, V. & Yoshida, K. (2014). Microdiamond discovered in the Seve Nappe (Scandinavian Caledonides) and its exhumation by the "vacuum-cleaner" mechanism. *Geology* **42**, 1107–1110.

Mercy, E. L. P. & O'Hara, M. J. (1965). Chemistry of some garnet-bearing rocks from south Norwegian peridotites. *Norsk Geologisk Tiddskrift* **445**, 323–332.

Moore, A. C. & Kvale, H. (1977). Three varieties of alpine-type ultramafic rocks in the Norwegian Caledonides and Basal Gneiss Complex. *Lithos* **10**, 149–161.

Nickel, K. G. & Green, D. H. (1985). Empirical geothermobarometry for garnet peridotites and implications for the nature of the lithosphere, kimberlites and diamonds. *Earth and Planetary Science Letters* **73**, 158–170.

Obata, M. (2011). Kelyphite and symplectite: textural and mineralogical diversities and universality, and a new dynamic view of their structural formation. In: Sharkov, E. V. (ed.) *New Frontiers in Tectonic Research*, London: IntechOpen, pp. 93–122.

O'Neill, H. Ste. (1981). The transition between spinel lherzolite and garnet lherzolite, and its use as a geobarometer. *Contributions to Mineralogy and Petrology* **77**, 185–194.

Osland, R. (1997). Modeling of variations in Norwegian olivine deposits, causes of variation and estimation of key quality factors. Doktor Ingeniør thesis, Norwegian University of Science and Technology, pp. 189. Ph.D. thesis, Norges Tekniske Høgskole, pp. 1–189.

Sahlstein, T. G. (1935). Petrographie der Eklogiteinschliisse in den Gneisen des sudwestlichen Liverpool-Landes in Ost-Grönland. *Meddelelse Grönland* **95**, 1–43.

Scambelluri, M., Van Roermund, H. L. M. & Pettke, T. (2010). Mantle wedge peridotites: fossil reservoirs of deep subduction zone processes Inferences from high and ultrahigh-pressure rocks from Bardane (Western Norway) and Ulten (Italian Alps). *Lithos* **120**, 186–201.

Smith, D. C. & Cheeney, R. F. (1981). A new occurrence of garnet-ultrabasite in the Caledonides; a Cr-rich chromite–garnet-lherzolite from Tvaerdalen, Liverpool Land, East Greenland. *Terra Cognita* **1**, 74.

Spengler, D., Brueckner, H. K., van Roermund, H. L. M., Drury, M. R. & Mason, P. R. D. (2009). Long-lived, cold burial of Baltica towards 200 km depth. *Earth and Planetary Science Letters* **281**, 27–35.

Spengler, D., van Roermund, H. L. M., Drury, M. R., Ottolini, L., Mason, R. D. & Davies, G. R. (2006). Deep origin and hot melting of an Achaean orogenic peridotite massif in Norway. *Nature* **440**, 913–917.

Su, B., Chen, Y., Guo, S. & Liu, J. (2016). Origins of orogenic dunites: petrology, geochemistry and implications. *Gondwana Research* **29**, 41–59.

Terry, M. P., Robinson, P., Brueckner, H. K. (1999). Sinking intrusion model for the emplacement of garnet-bearing peridotites into continental collision orogens: comment and reply. *Geology* **27**, 447–448.

Van Roermund, H. L. M. (2009a). Recent progress in Scandian UHPM in the northernmost domain of the Western Gneiss Complex, SW Norway: continental subduction down to 180–200 km. *Journal of the Geological Society of London* **166**, 1–13.

Van Roermund, H. L. M. (2009b). Mantle wedge garnet peridotites from the northernmost ultra-high pressure domain of the Western Gneiss Region, SW Norway. *European Journal of Mineralogy* **21**, 1085–1096.

Wang, Q., Xia, Q.-K., O'Reilly, S. Y., Griffin, W. L., Beyer, E. E. & Brueckner, H. K. (2013). Pressure- and stress-induced fabric transition in olivine from peridotites in the Western Gneiss Region (Norway): implications for mantle seismic anisotropy. *Journal of Metamorphic Geology* **31**, 93–111.

Wu, C. M., & Zhao, G. C. (2007). A recalibration of the garnet-olivine geothermometer and a new geobarometer for garnet peridotites and garnet-olivine-plagioclase-bearing granulites. *Journal of Metamorphic Geology* **25**, 497–505.